

Fold and fabric relationships in temporally and spatially evolving slump systems: A multi-cell flow model



G. Ian Alsop^{a,*}, Shmuel Marco^b

^a Department of Geology and Petroleum Geology, School of Geosciences, University of Aberdeen, UK

^b Department of Geophysics and Planetary Sciences, Tel Aviv University, Tel Aviv 69978, Israel

ARTICLE INFO

Article history:

Received 2 December 2013

Received in revised form

14 February 2014

Accepted 19 February 2014

Available online 4 March 2014

Keywords:

Slump folds

Foliation

Mass Transport Complex

Dead Sea

ABSTRACT

Folds generated in ductile metamorphic terranes and within unlithified sediments affected by slumping are geometrically identical to one another, and distinguishing the origin of such folds in ancient lithified rocks is therefore challenging. Foliation is observed to lie broadly parallel to the axial planes of tectonic folds, whilst it is frequently regarded as absent in slump folds. The presence of foliation is therefore often considered as a reliable criterion for distinguishing tectonic folds from those created during slumping. To test this assertion, we have examined a series of well exposed slump folds within the late Pleistocene Lisan Formation of the Dead Sea Basin. These slumps contain a number of different foliation types, including an axial–planar grain-shape fabric and a crenulation cleavage formed via microfolding of bedding laminae. Folds also contain a spaced disjunctive foliation characterised by extensional displacements across shear fractures. This spaced foliation fans around recumbent fold hinges, with kinematics reversing across the axial plane indicating a flexural shear fold mechanism. Overall, the spaced foliation is penecontemporaneous with each individual slump where it occurs, although in detail it is pre, syn or post the local folds. The identification of foliations within undoubted slump folds indicates that the presence or absence of foliation is not in itself a robust criterion to distinguish tectonic from soft-sediment folds. Extensional shear fractures displaying a range of temporal relationships with slump folds suggests that traditional single-cell flow models, where extension is focussed at the head and contraction in the lower toe of the slump, are a gross simplification. We therefore propose a new *multi-cell flow model* involving coeval second-order flow cells that interact with neighbouring cells during translation of the slump.

© 2014 Elsevier Ltd. All rights reserved.

1. Introduction

A perennial problem when working in ancient deformed sedimentary rocks is clearly separating and distinguishing structures generated within unlithified “soft-sediment” from those folds and fabrics that developed during subsequent deformation of the fully lithified rock (e.g. Elliot and Williams, 1988; Maltman, 1984, 1994a,b,c; Debacker et al., 2006; Ortner, 2007; Waldron and Gagnon, 2011). A particularly perplexing issue relates to determining the origin of folds that are widespread features in a range of both tectonic and sedimentary environments. The presence of axial planar cleavage in tectonic folds, compared to its absence in soft-sediment folds, has been quoted in older texts as a robust and reliable criterion for distinguishing tectonic folds from slump folds

(e.g. Potter and Pettijohn, 1963). As such, Webb and Cooper (1988, p.470) note that “characteristic slump related features include ... tight to isoclinal folds with no related cleavage”. Indeed, a number of recent text books, including that of Fossen (2010, p.239), perpetuate this view and note that soft-sediment folds “generally lack the axial planar cleavage so commonly associated with folds formed under metamorphic conditions.”

However, the counter-argument that cleavage, which is defined as “the ability of a rock to split or cleave into more or less parallel slices”, or foliation, defined as “any fabric-forming planar or curvilinear structure” (Fossen, 2010, p.244–245) may in fact form apparently axial–planar fabrics to sedimentary slump folds has also long been suggested and debated (e.g. Williams et al., 1969; Corbett, 1973; Woodcock, 1976a,b; Tobisch, 1984; McClay, 1987; Farrell and Eaton, 1988; Maltman, 1994c). Two principle models have been proposed to explain how such sedimentary fabrics may develop with apparent axial–planar relationships to slump folds (see Maltman, 1981; Tobisch, 1984; Elliot and Williams, 1988). In

* Corresponding author.

E-mail address: Ian.Alsop@abdn.ac.uk (G.I. Alsop).

the first interpretation, the authors of some text books (e.g. Price and Cosgrove, 1990, p. 455) claim that cleavages that appear to be axial–planar with respect to sedimentary slump folds may actually be later and reflect mimetic growth of minerals during subsequent diagenesis of the sediment. This view is supported in a more recent text book, where Passchier and Trouw (2005, p.245) compare folds formed in tectonically deformed rocks with those generated in soft-sediments and note that “an obvious difference is that no axial plane cleavage should be present (in slump folds), but diagenetic foliation may have formed, parallel to bedding and axial planes”.

A second interpretation has proposed that sub-horizontal foliations that are apparently axial–planar to flat-lying recumbent slump folds are actually created by compaction of the sediment during subsequent burial and lithification (see discussion in Maltman, 1994c; McClay, 1987, p.12). The horizontal compaction fabric is thus fortuitously parallel to the axial plane of the recumbent slump fold. Consequently, both interpretations described above invoke a phase of subsequent foliation development that is parallel to the axial plane of the earlier slump fold. Maltman (1994d, p.153) summarised this dilemma for the relationship between slump folds and adjacent fabrics by noting “As yet, there is no good record of a slump fold with an axial–plane foliation that definitely formed through slumping rather than consolidation, but the question remains open”.

Clearly the range of potential interpretations regarding slump fold and foliation relationships noted above is important because they can critically alter the fundamental understanding of the timing between sedimentation and deformation patterns. The interpretation of sedimentary environments and associated palaeogeographies, not to mention isotopic dating of intrusions that postdate *apparently* regional structures, are seriously flawed if the basic field relationships associated with recognition of soft-sediment deformation are incorrectly identified. Debate continues on the timing of regional deformation relative to lithification, with the possibility that pockets of overpressured sediment may remain unlithified for periods of time whilst surrounding areas are lithified and undergo “tectonic” deformation (e.g. Phillips and Alsop, 2000; Ortner, 2007; see Waldron and Gagnon, 2011). While regional deformation could strike at any stage within the spectrum of the continuing lithification process, resulting in a degree of ambiguity as to whether folds and foliations were forming in truly “soft-sediment”, the generation of slump folds requires the sediment to be unlithified *at the time of slumping* and thereby negates much of that debate.

In addition to the potential pitfalls in regional correlation and dating of deformation events outlined above, the study of foliation development and deformation in unlithified sediments, in general, is also significant because of the profound effects it may have on the permeability of the host sediment. This possibility has obvious implications for hydrocarbons and fluid flow (e.g. Hurst et al., 2011). Furthermore, the study and interpretation of fabrics associated with soft-sediment deformation is important for the recognition and understanding of ancient Mass Transport Complexes (MTC's) that are increasingly interpreted from offshore seismic sections and are growing in economic significance (e.g. see review by Lee et al., 2007; Bull et al., 2009; Jackson, 2011). Understanding the development of cleavages and foliations is crucial because they are sub-seismic scale deformation that is “hidden” on seismic sections, but are important to the deformation analysis. As such, foliation may be a manifestation of lateral compaction, that could account for up to 40% “shortening” that is apparently absent, but is required to balance and restore regional cross sections in offshore MTC's (e.g. see Butler and Paton, 2010). Finally, the study of foliation in sediment is of more general interest because it may be useful when interpreting folds and fabrics in

other settings and environments where flow occurs such as sub-glacial shear zones (e.g. Lesemann et al., 2010; Pisarska-Jamrozko and Weckwerth, 2012 and references therein) or salt flows (e.g. Aftabi et al., 2010).

Central to many of these arguments is the basic issue as to whether foliations can indeed form genuine axial–planar fabrics to slump folds created during soft-sediment deformation. To address this fundamental problem, we have therefore undertaken a detailed study involving observations of both foliations and slump folds in an attempt to better understand their geometry and relationships to one another. The aim of this contribution is therefore to clarify if a) foliations can form axial–planar to slump folds, and if so, b) the nature and kinematic significance of such fabrics in models of slump systems. In particular we raise a number of important questions including:

- i) What are the different types of foliations and lineations that may form around slump folds?
- ii) What are the relative timing relationships between foliations and slump folds?
- iii) What are the kinematics associated with sedimentary foliation development?
- iv) What relationship, if any, does the orientation of foliation have with the slope?
- v) Can foliation–bedding relationships be used to distinguish sedimentary and tectonic folds?
- vi) How can the development of foliation be incorporated into models of flow within slumps?

Although a number of authors have previously described apparent axial–planar fabrics from slump folds (e.g. Williams et al., 1969; Bell, 1981; Tobisch, 1984), the detailed relationships are frequently hindered by the analyses being undertaken in ancient rocks that have experienced subsequent diagenesis and tectonism (see Elliot and Williams, 1988). These younger events may alter, mask, or even entirely overprint the original relationships, creating ambiguity in these interpretations. Many of these issues about ambiguity from overprinting are absent from the late-Pleistocene Lisan Formation developed around the Dead Sea Basin. Superb preservation, coupled with the option of 3-D excavation in these largely unlithified sediments, allows us to examine a range of fold-related structures such as grain-shape fabrics, crenulation cleavage, spaced foliations and intersection lineations that normally are restricted to analysis in classical metamorphic rocks (e.g. Turner and Weiss, 1963; Ramsay, 1967; Ramsay and Huber, 1987).

2. Soft-sediment deformation

Over the past 40 years, gravity-driven slumps of unconsolidated sediment have typically been modelled in terms of deformation cells translating downslope (e.g. Hansen, 1971; Lewis, 1971; Farrell, 1984). These systems are marked by extension in the upslope portion of the slump that is broadly balanced by contraction in the downslope or toe area of the slump (e.g. Farrell, 1984; Farrell and Eaton, 1987; Elliot and Williams, 1988; Martinsen, 1989, 1994; Martinsen and Bakken, 1990; Smith, 2000; Debacker et al., 2001; Strachan, 2002, 2008; Gilbert et al., 2005; Garcia-Tortosa et al., 2011) (Fig. 1). Within such models, translation of the slump–sheet occurs along some form of underlying detachment or failure surface with extension at the head accommodated by normal faults and fractures, while folds are considered to be one of the primary manifestations of contraction in the lower portion of the slump (e.g. see review in Alsop and Marco, 2011) (Fig. 1). Deformation associated with translation along the basal decollement is considered to be dominated by non-coaxial strain (e.g. Wetzler et al., 2010),

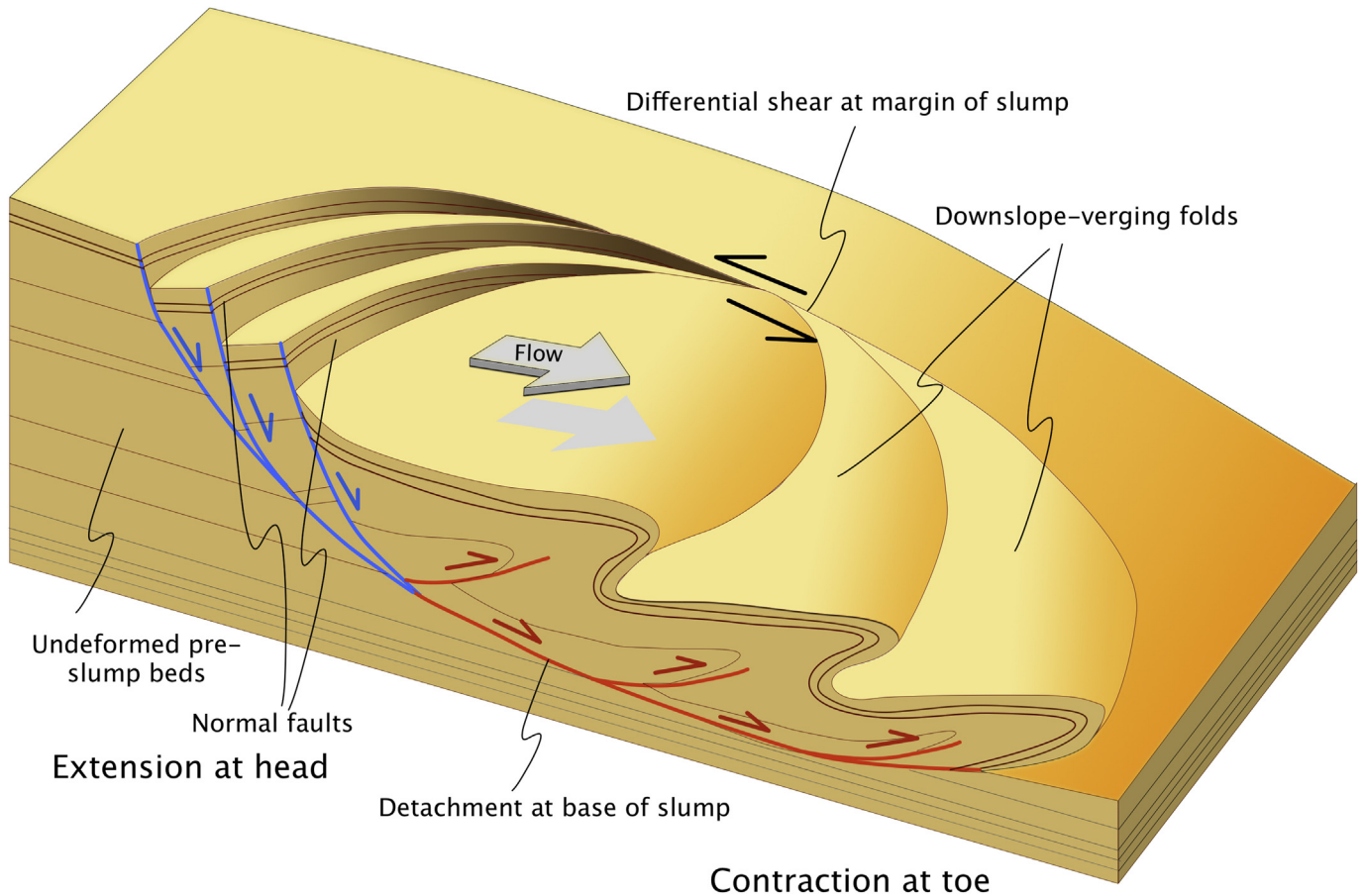


Fig. 1. Schematic 3D cartoon illustrating gravity-driven downslope slumping of sediments above a basal detachment, marked by extensional normal faults at the upslope head, and contractional folds and thrusts at the downslope toe. Lateral margins of the slump are interpreted to reflect differential strike-slip shear.

whereas the overlying portions of each slump are modelled as reflecting an increasing component of pure shear (e.g. Webb and Cooper, 1988). The lateral margins of the slump are interpreted to be zones of differential shear that are broadly parallel to overall downslope-directed movement (e.g. Farrell, 1984; Debacker et al., 2009) (Fig. 1). The general temporal evolution of slump systems is initiation, translation, cessation, relaxation and compaction of the slump-sheet (Farrell, 1984; Strachan, 2002, 2008; Alsop and Marco, 2011).

In the most simple slump-sheet scenario, the hinges of slump folds are orientated normal to the slope direction, with axial planes dipping in the upslope direction and the overall slump fold system verging downslope (e.g. Woodcock, 1979; Bradley and Hanson, 1998) (Fig. 1). This simple geometry is replaced with increasing deformation during progressive translation of the slump, whereby fold hinges may rotate towards the downslope direction to create curvilinear sheath folds (e.g. Allen, 1984; Farrell and Eaton, 1987, 1988; Alsop and Carreras, 2007; McClelland et al., 2011; Alsop and Holdsworth, 2012; Alsop and Marco, 2013), or alternatively hinges may detach and roll downslope to create spiral folds (Alsop and Marco, 2013; Allen, 1984, p.382).

Differential shear at the lateral margins of slump-sheets may generate folds that actually initiate at variable angles to the slope direction, leading to distinct relationships between fold hinge and axial plane orientation, vergence, and the downslope direction (see Alsop and Holdsworth, 2007; Debacker et al., 2009; Alsop and Marco, 2012a). Overall, the resulting complexity created from folds initiating at a variety of orientations, or undergoing variable

amounts of rotation and/or rolling downslope may be viewed as part of a single progressive deformation during continued translation of the slump-sheet (Alsop and Holdsworth, 2007). The relationships that foliations display to slump folds within this traditional dislocation model of Farrell (1984), and the key role they undertake in overall deformation of the slump system has not been previously discussed in detail.

3. Regional setting

The Dead Sea Basin is a pull-apart basin developed between two parallel fault strands that define the Dead Sea transform (Garfunkel, 1981; Garfunkel and Ben-Avraham, 1996) (Fig. 2). The transform has been active since the Miocene (e.g. Bartov et al., 1980; Garfunkel, 1981) including during deposition of the Lisan Formation in the late Pleistocene (70–15 ka) (Haase-Schramm et al., 2004). This transform has produced numerous earthquakes that trigger soft-sediment deformation and slumping in the Lisan Formation (e.g. see Alsop and Marco, 2011).

The Lisan Formation comprises a sequence of fine couplets defined by alternating aragonite-rich and clastic-rich laminae on a sub-mm scale. They are thought to represent annual varve-like cycles with aragonite-rich laminae precipitating from hypersaline waters in the hot dry summer, while winter flood events wash clastic material into the lake to form the detrital-rich laminae (Begin et al., 1974). Seismic events along the Dead Sea Transform are considered to trigger surficial slumps within the Lisan Formation, resulting in well-developed soft-sediment fold and thrust

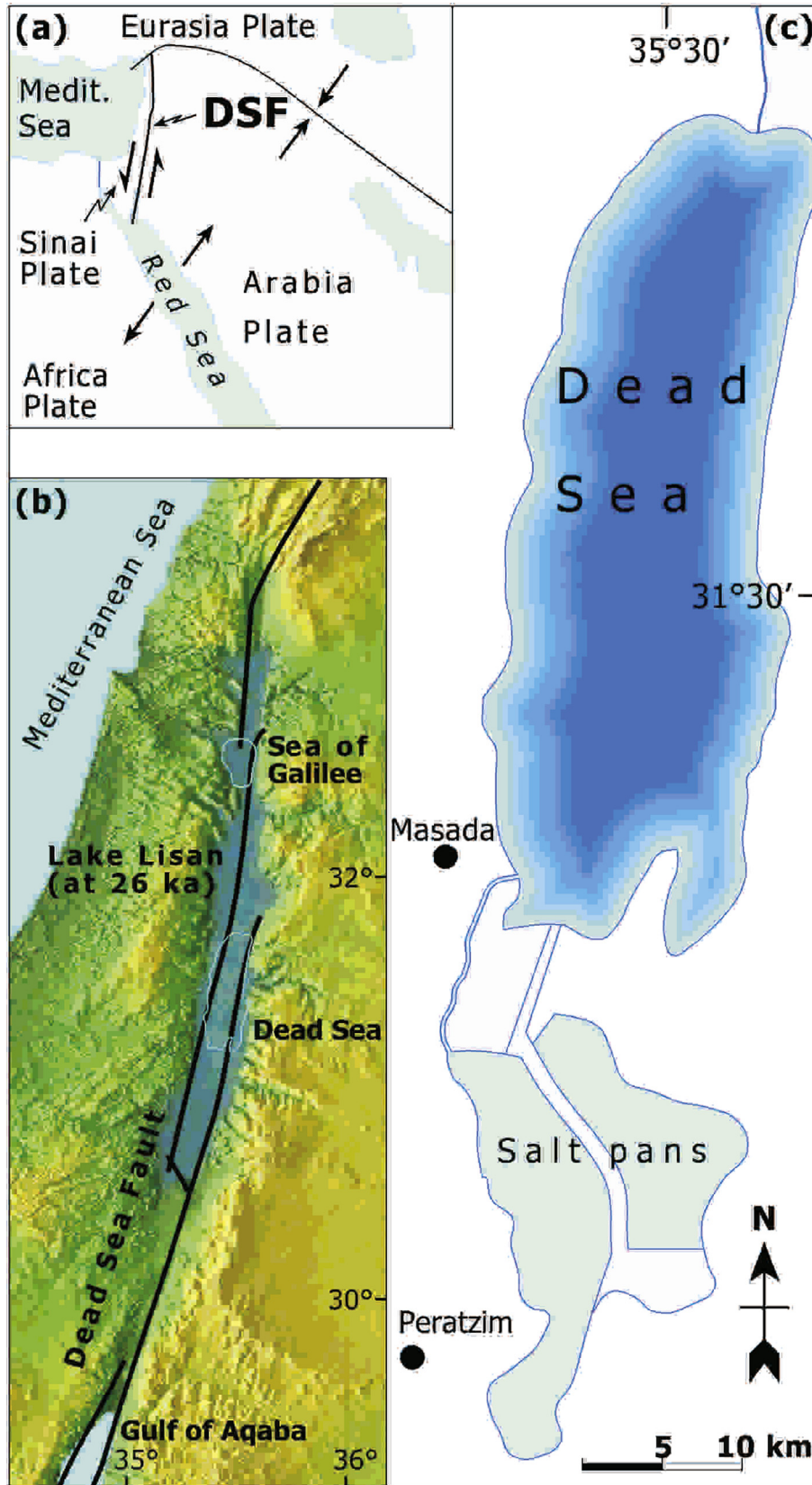


Fig. 2. Map of the Dead Sea and localities referred to in the text a) Tectonic plates in the Middle East. General tectonic map showing the location of the present Dead Sea Fault (DSF). The Dead Sea Fault transfers the opening motion in the Red Sea to the Taurus-Zagros collision zone. b) Generalised map showing the maximum extent of Lake Lisan along the Dead Sea Fault at 26 ka. c) Map of the Dead Sea showing the position of Masada and the case study area of Peratzim.

systems (Alsop and Marco, 2011). Breccia layers generated next to syn-depositional faults are thought to be the product of seismicity (e.g. Marco and Agnon, 1995; Agnon et al., 2006). Detrital (mud-rich) horizons that are <10 cm thick and contain fragments of aragonite laminae are interpreted to be deposited from suspension also following seismicity (e.g. Alsop and Marco, 2012b). Individual slump-sheets are typically <1.5 m thick and are capped by undeformed horizontal beds of the Lisan Formation.

The slumps together with the intervening undeformed beds within the Lisan Formation are cut by vertical sedimentary injections containing fluidised sediment sourced from underlying units (e.g. Marco et al., 2002; Levi et al., 2006). Within the sedimentary injections, optically stimulated luminescence (OSL) ages of quartz give ages of between 15 and 17 ka (Porat et al., 2007), indicating brittle failure and intrusion after deposition of the Lisan Formation during 70–15 ka (Haase-Schramm et al., 2004). The slump systems around the Dead Sea Basin are developed on very gentle slopes of <1° dip and define an overall regional pattern of radial slumping directed towards the deponent centre of the present Dead Sea Basin (Alsop and Marco, 2012b, 2013).

4. General observations from the study area

We have examined different parts of the slump system exposed via a series of wadi cuttings at Peratzim in the southern Dead Sea Basin (N31° 0449.6, E35° 2104.2) (see Alsop and Marco, 2011). Individual cuttings typically extend for up to 1 km, with vertical walls up to 5 m high. This topography results in reasonably continuous exposure through the lower parts of the slump system, with only limited areas masked by local wall collapse. Slump folds at Peratzim are typically <1 m wavelength and occur in horizons that are normally <1.5 m thick (Figs. 3–5). Folds are upright to recumbent, with sub-horizontal rounded rather than angular hinges. Folds are NW–SE trending, typically verge (89%) towards the NE and are associated with axial planes dipping variably towards the SW (Alsop and Marco, 2011). NE-verging folds and thrusts typically detach on underlying thin (<10 cm thick) mud-rich horizons that appear to have acted as weak décollements (Alsop and Marco, 2013). Fold facing is directed towards 042°, whereas axial planes generally strike 126° suggesting a palaeoslope directed towards 036°, although steeper (>45°) axial-planar strike (that may more accurately reflect palaeoslope) indicate a direction towards 034° (Alsop and Marco, 2011, see Strachan and Alsop, 2006; Lesemann et al., 2010 for methodology). A combination of methods suggests that the palaeoslope and direction of slumping of sediments was towards 040° (Alsop and Marco, 2012a).

Our previous examinations (Alsop and Marco, 2011, 2012a,b, 2013) reveal that a) slump folds and associated structures are truncated by an overlying erosive surface; b) the eroded slump is covered by a thin (typically <10 cm thick) clastic horizon that displays upward-fining graded bedding formed when this unit was deposited out of suspension; c) this clastic horizon, together with overlying beds display marked thickening and thinning to infill local bathymetry created by the slump (see Alsop and Marco, 2013) and d) slumps within the Lisan Formation at Peratzim are overlain by up to just 6 m of Lisan Formation, which are capped by a further 1–2 m of Holocene alluvium. The total thickness of overburden therefore typically never exceeded 8 m meaning that the Lisan marls are poorly consolidated. These observations collectively demonstrate that a sedimentary or ‘welded contact’ developed above the slump and indicate that a) the deformation is intraformational and related to slumping; and b) the slump must have formed at the sediment surface rather than being buried

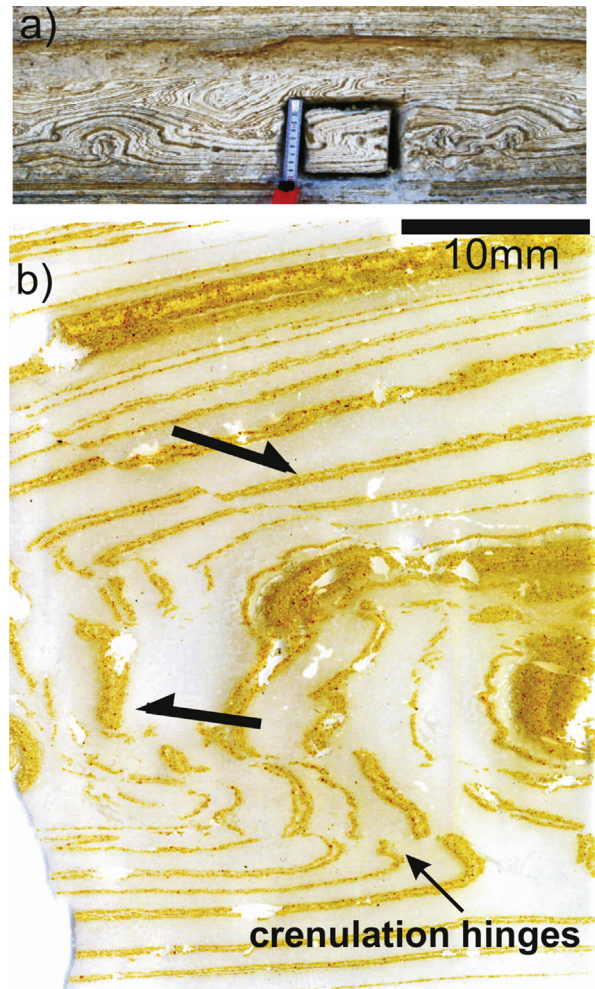


Fig. 3. Field photograph (a) and associated photomicrograph (b) of micro-scale folding and shear fractures within the Lisan Formation from Masada (see location on Fig. 2c). The image shows light coloured aragonite-rich laminae separated by darker clay-rich seams, that have been subsequently folded and fractured during soft-sediment slumping. A right-stepping extensional fracture is developed on the upper limb of the fold (marked by the arrow translating to the right), and contractional fractures form in the thickened hinge and short limb (translating to the left). West is on the left and east on the right of the photographs.

beneath a thickness of overburden. This inference is significant as any foliations and fabrics directly associated with the folds must therefore have also formed during slumping at the sediment surface.

Details of folds and foliations were examined via thin sections from within the Lisan Formation exposed at Masada (Fig. 2c). These sections show relatively continuous laminae developed with mm-scale spacing (Fig. 3a and b). These laminae are subsequently folded and display crenulations in fold hinges, with aragonite-rich laminae showing a relative thickening in the hinge compared to limbs, suggesting that these units were relatively weak and able to flow (Fig. 3b). The laminae are cut by cm-scale contractional and extensional shear fractures, defined as ‘discontinuities in displacement or mechanical properties’ marked by ‘fracture parallel slip’ (Fossen, 2010, p.124). Such shear fractures locally intensify in the hinges of folds to define spaced axial-planar foliation planes (Fig. 3b). Difficulties in preparing thin sections from unconsolidated sediments precluded further analysis. However, this limited investigation does illustrate the detailed nature of the aragonite and clastic laminae, and

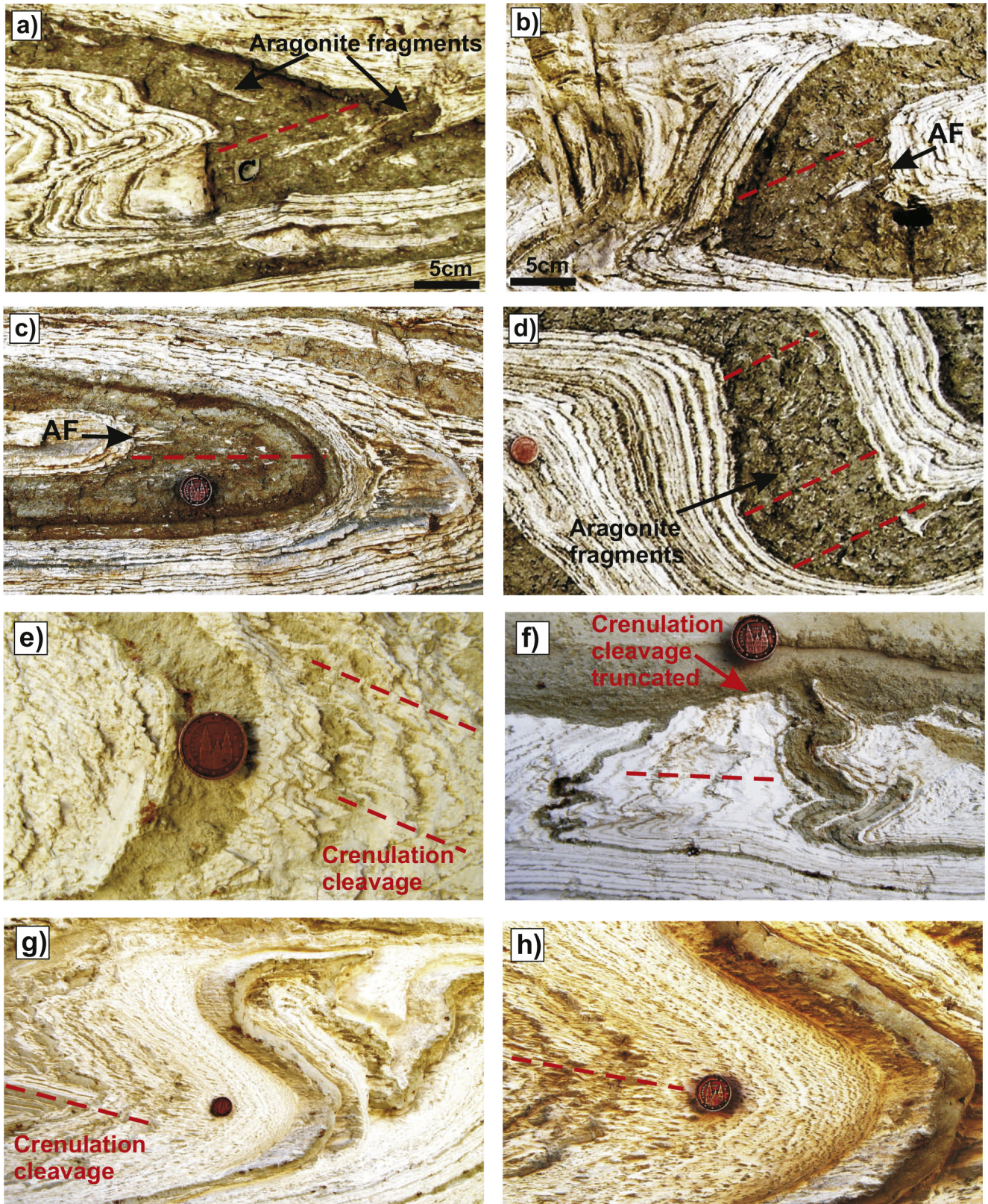


Fig. 4. a–d) Photographs of axial–planar grain-shape fabrics defined by aragonite fragments (AF) in detrital mud-rich horizons of the Lisan Formation at Peratzim. Aragonite fragments were deposited sub-parallel to bedding, and were subsequently rotated to lie parallel to fold axial planes. e–h) Crenulation cleavage formed in aragonite-rich beds with mm-scale bedding laminae. Red dashed lines define orientation of grain-shape fabric (a–d) and crenulation cleavage (e–h). Crenulation cleavages form axial–planar to slump folds truncated by overlying erosive unconformities (f), or in refolds created during continued slump movement (g). Coin has 15 mm diameter. West is on the left and east on the right of the photographs. (For interpretation of the references to color in this figure legend, the reader is referred to the web version of this article.)

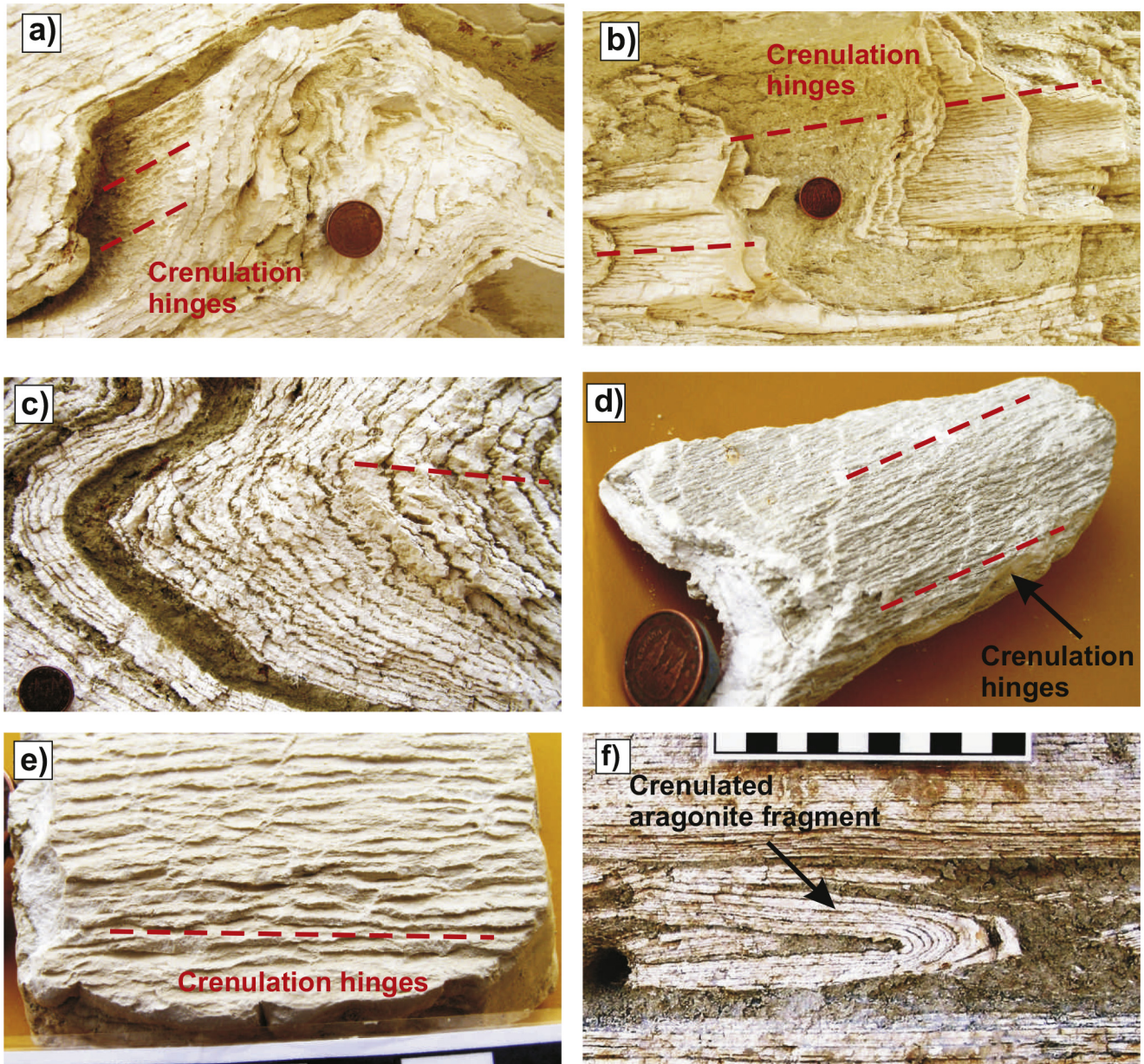


Fig. 5. a–f) Photographs of crenulation hinges developed on a mm-scale in the laminated aragonite and clastic-rich layers of the Lisan Formation at Peratzim. a–d) Minor crenulation axes are sub-parallel to associated fold hinges and locally anastomose with one another (e). Red dashed lines define orientation of crenulation hinges. Crenulation hinges may form within slump folds that become entirely detached and redeposited in overlying clastic horizons (f). Coin has a 15 mm diameter and in (e) scale divisions are 1 cm. West is on the left and east on the right of the photographs. (For interpretation of the references to color in this figure legend, the reader is referred to the web version of this article.)

demonstrate that slump folds are associated with a range of crenulations and foliations that form the basis of this investigation.

5. Detailed observations of soft-sediment cleavage geometries

Superb examples of sedimentary folds developed in a series of slump-sheets are preserved at Peratzim. The slumped horizons containing folds are typically <1.5 m thick, while the intervening sequence is undeformed. The varve-like layering of the aragonite and clastic-rich laminae enables the preservation and recording of exceptionally fine structural minutiae. These details include a range of cleavages and foliations that are related to either local contraction or extension.

5.1. Foliations related to contraction

5.1.1. Axial–planar grain-shape fabric

Within the Lisan Formation, thicker (<10 cm) clastic layers comprising detrital mud and containing aragonite fragments (1–2 mm in length) are considered to be formed by deposition from suspension following seismic events (e.g. Marco and Agnon, 1995; Agnon et al., 1996; Alsop and Marco, 2012b). Coarser aragonite fragments, up to 5 cm in length, are typically tabular in shape reflecting the inherent anisotropy of the laminae, and are deposited with the long axis of the clast aligned sub-parallel to the horizontal bedding (Fig. 4a). Layers containing these fragments may be folded and deformed during subsequent slumping events. Within the hinges of slump folds, the elongate fragments become reorientated such that they lie oblique to bedding and parallel to the horizontal

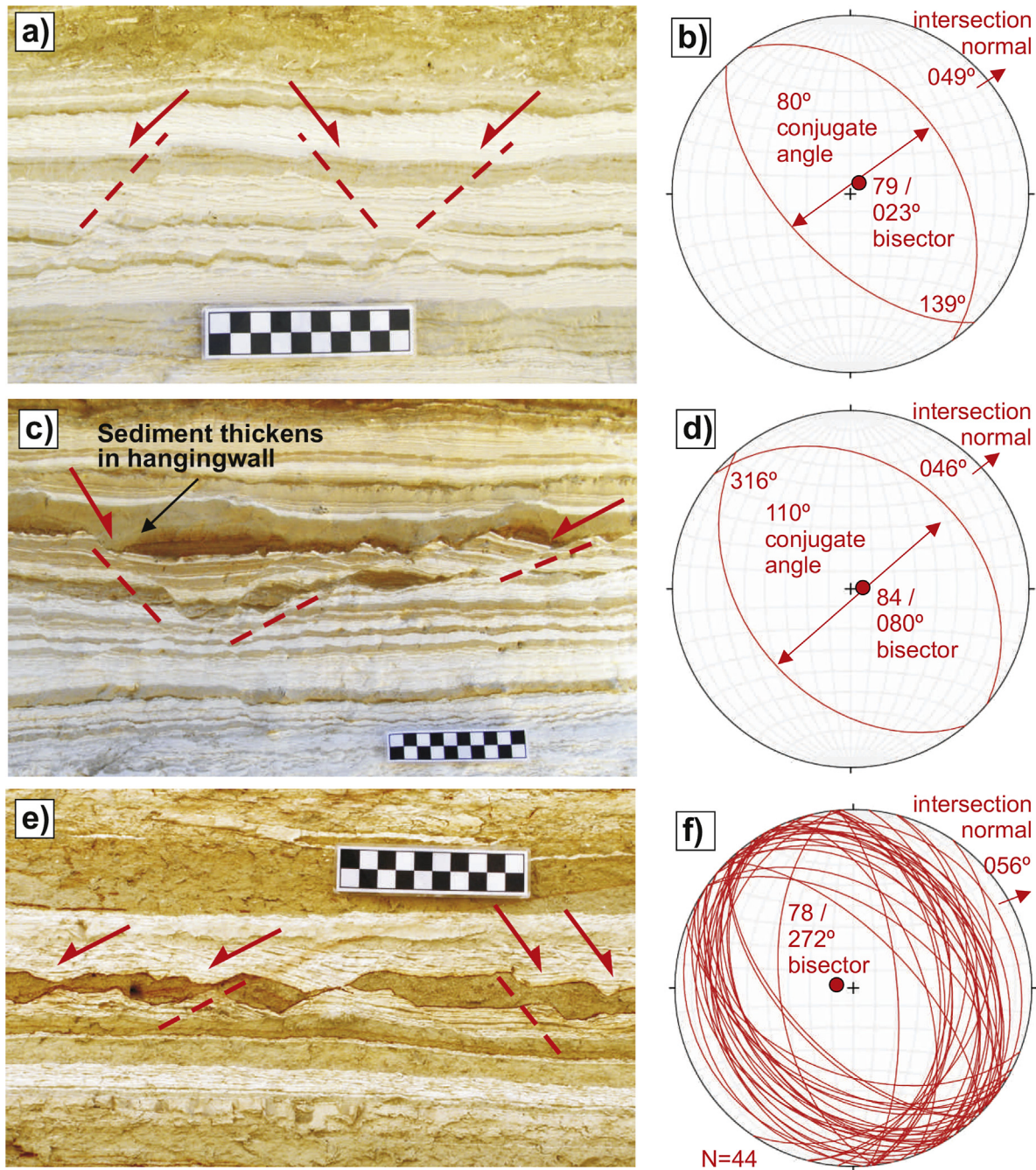


Fig. 6. a–d) Photographs and associated stereonet pairings of NW–SE trending conjugate shear fractures. e) Conjugate shear fractures. f) stereonet of all extensional shear fractures. Red dashed lines define orientation of fracture planes, while conjugate angles, orientation of bisectors and intersection normals are shown on stereonets. Scale bar is 10 cm. West is on the left and east on the right of the photographs. (For interpretation of the references to color in this figure legend, the reader is referred to the web version of this article.)

or gently dipping axial plane of the fold (Fig. 4a–d). The grain-shape fabric defined by aragonite fragments is typically sub-horizontal, although it may dip at angles of up to 28° (Fig. 4d). This axial–planar fabric is parallel to a crenulation cleavage that is developed in the adjacent aragonite-rich laminae (Fig. 4c and d).

5.1.2. Crenulation cleavage

Contractional crenulations developed on a mm-scale are abundant within folds of the Lisan Formation (Fig. 4e–h). Crenulations are either symmetric or asymmetric, and collectively define a zonal crenulation cleavage that is broadly axial–planar to associated folds (Fig. 4e–h). The crenulation cleavage locally intensifies in fold

hinges to create a discrete crenulation cleavage where discontinuities have formed (Fig. 4e). The crenulation cleavage is best developed in finely laminated aragonite-rich layers where dark detrital laminae form well defined markers that are clearly crenulated (Figs. 4f and 3b). It is these depositional couplets that form an extremely fine (<1 mm spacing) layer-cake laminae that allow the preservation of a crenulation cleavage. Crenulation cleavage is not observed in the thicker detrital and mud-rich units that lack fine depositional laminations (Fig. 4e and f).

It is notable that crenulation cleavages are formed axial–planar to refolded folds, generated during continued slump movement (Fig. 4g and h). In addition, folds with axial–planar crenulation

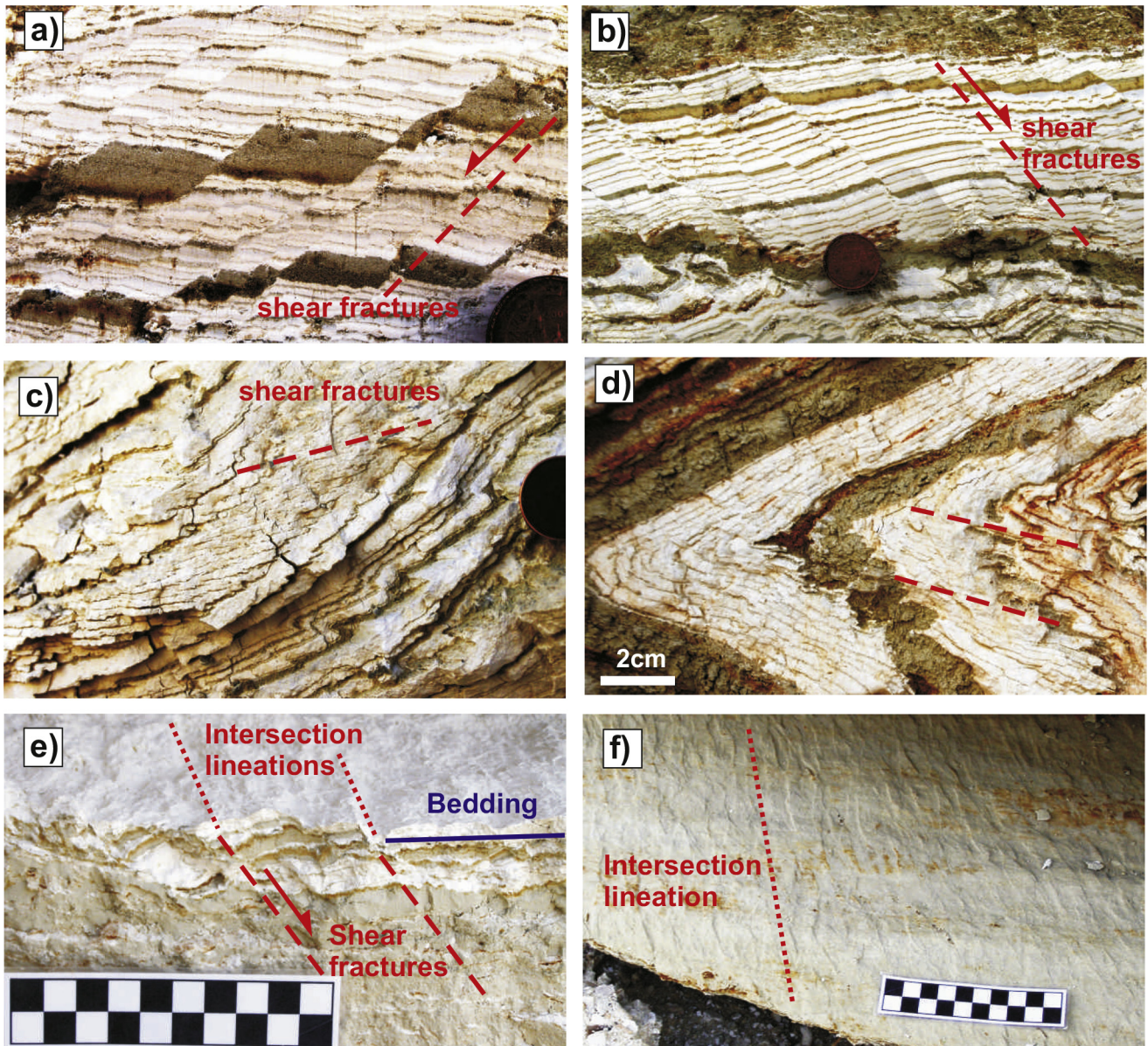


Fig. 7. Photographs of extensional shear fractures (a–d) and associated intersection lineations (e–f). Shear fractures may locally intensify to create a foliation (c) that is axial–planar to associated folds (d). Extensional shear fractures intersect bedding planes as a series of stepped surfaces spaced at a mm–cm scale (e, f). Coin has a 15 mm diameter and scale bar is 10 cm. West is on the left and east on the right of the photographs.

fabrics are themselves truncated by overlying erosive unconformities (Fig. 4f). These relationships conclusively demonstrate that crenulation cleavage forms at the time of slumping and is not a later superimposed fabric.

5.1.3. Crenulation lineations

Crenulation lineations are defined by the hinge lines of microfolds (Passchier and Trouw, 2005 p.101) and are created when the hinges of mm-scale microfolds become aligned with one another. Within the Lisan Formation, the troughs and crests are defined by the folded aragonite-rich laminae, and are typically best developed in the hinge and short limbs of larger host folds (Fig. 5a–c). Overall, crenulation lineations trend ENE or NE sub-parallel to the fold hinges and are associated with crenulation cleavage (Fig. 5a, b, d). In detail, troughs and crests may anastomose over mm–cm scales when traced along the length of their hinges (Fig. 5d and e).

Woodcock (1976b) originally noted that lineations were parallel to fold hinges, and the alignment of crenulations with associated fold hinges in the present study indicates that they formed at the same time. In some extreme cases, folded aragonite layers with an axial–planar crenulation cleavage become entirely detached and incorporated into the clastic layer that was deposited from suspension above the erosive unconformity (Fig. 5f) This geometry is important because it once again demonstrates that crenulations formed at the time of slumping (i.e. pre-erosive contact) and are not a later superimposed fabric.

5.2. Foliation related to extension

5.2.1. Shear fractures

Extensional shear fractures developed with a mm–cm scale spacing are observed locally within the finely laminated aragonite-rich layers, and appear similar to ‘microfaults’ in slumped

sediments (Farrell, 1984). The shear fractures are typically NW–SE striking with moderate dips towards either the SW or NE (Fig. 6a–f). Shear fractures consistently display an extensional displacement of bedding, and their relative offsets indicate that they are coeval independent of dip direction (Fig. 6a–d). Shear fractures resulting in extensional offset and back-rotation of bedding are locally marked by thickening of the sedimentary package in their hangingwall (Fig. 6c). These small-scale growth geometries are important as they reflect shear fractures influencing patterns of sedimentation, thereby indicating fractures formed at or near the sediment surface. The shear fractures display an overall conjugate pattern, with the bisector to the conjugate centred about the vertical (Fig. 6b, d). The normal to the SE trending intersections is directed towards the NE (056°) sub-parallel to the inferred (040°) palaeoslope direction (Fig. 6f) (Alsop and Marco, 2012b).

The spacing between shear fractures is variable and increases to ~ 1 cm as it passes through thicker (~ 1 cm) aragonite and detrital-rich horizons (Fig. 7a–c). However, within the hinges of some slump folds, the spacing between shear fractures reduces to <5 mm such that it may be termed a strong axial–planar foliation (Fig. 7d). The shear fractures are defined by very thin (<0.1 mm) zones of displacement that are variably oblique to bedding, and collectively display a consistent sense of extensional offset of bedding (Fig. 7a and b). The shear fractures also locally offset the crenulation lineation, indicating that the fractures developed slightly later during slumping.

5.2.2. Intersection lineations

Shear fractures and bedding are typically oblique to one another and therefore create intersection lineations (Fig. 7e and f). Such spaced fractures produced during soft-sediment deformation, together with their associated intersection lineations, were described previously by Farrell and Eaton (1988). The mm–cm scale spacing of the shear fractures create intersections on bedding surfaces of similar spacing that may locally offset the bedding to form anastomosing spaced steps (Fig. 7e and f). The steps demonstrate that the fracture has undergone slip and displacement on a mm-scale (Fig. 7e). In general, the slip is extensional relative to bedding apart from where the fracture and bedding were both subsequently reorientated around later slump folds (see section 6.1).

In general, shear fracture intersection lineations plunge very gently towards the SE, and are parallel to associated fold hinges, indicating that the shear fractures define a foliation that is axial–planar or simply fans around the fold. The intersection lineations of the shear fractures displace crenulation lineations on bedding planes once again indicating that the fractures locally postdate the crenulation cleavage.

Thus, within the Lisan Formation, a pervasive axial–planar grain-shape fabric, together with a zonal crenulation cleavage are related to contractional deformation. Shear fractures are associated with extensional displacements, and may locally intensify within the hinges of slump folds to form axial–planar foliations.

6. Temporal relationships between shear fractures and slump folds

In order to further investigate shear fractures and intersection lineations around slump folds, we have undertaken excavations of a range of fold relationships within the Lisan Formation. Detailed observations reveal that the shear fractures display a variety of temporal associations to adjacent NE-verging slump folds. These observations are made within individual slumped horizons over a distance of few 10's metres at Peratzim. Importantly, no correlation

exists between the temporal relationships exhibited by folds and shear fractures and their overall position in the slump.

6.1. Pre-folding shear fractures

Within metamorphic terranes, foliation that is deformed and wrapped around folds is interpreted as reflecting an earlier foliation surface (S_1) being reworked by subsequent phases of folding (F_2). Thus, a clear temporal chronology for deformation can be developed locally by establishing such re-fold relationships.

The shear fractures are NW–SE striking and display moderate but variable dips towards the SW (Fig. 8a–c). In some cases, the shear fractures dip towards both the SW and then NE as they pass around the fold hinge (Fig. 8d–g). In such instances, shear fractures display systematic variations in offset around the hinges of NE-verging slump folds so that they display normal geometry on the upper fold limb and apparent reverse (contractional) displacement in the hinge and the lower limb. As the shear fractures display variable dips around the hinge of the fold, the bedding laminae in microlithons between fracture planes become noticeably oblique to mud-rich horizons defining bedding around the fold (Fig. 8a–g). This geometry suggests a degree of detachment along these detrital horizons.

Overall, the local preservation in the hinge of the fold of shear fractures with apparent thrust geometries surrounded by otherwise extensional offsets can be achieved through bulk rotation of the hinge and short fold limb and the shear fractures it contains. We therefore interpret this relationship as shear fractures pre-dating adjacent NE-verging slump folds.

6.2. Syn-folding shear fractures

Syn-folding foliation relationships are classically observed around tectonic folds where reversals in cleavage–bedding vergence are employed in the analysis of metamorphic terranes. Similar relationships are visible around slump folds of the Lisan Formation.

The syn-folding shear fractures are generally NW–SE striking and dip moderately towards either the SW or NE to define overall conjugate patterns (Fig. 9). Shear fractures are notably absent in the fold hinges, but are observed to abruptly switch orientations and kinematics on passing from the upper to the lower limb of the fold. SW-dipping shear fractures are developed on the long limbs of NE-verging folds with the fractures becoming NE-dipping on the associated short limbs (Fig. 9e–j). Thus, in fold pairs, up to 3 switches in orientation and sense of offset across shear fractures may occur on crossing from the long limb to short limb and back to the long limb (Fig. 9g and h). This reversal in kinematics can develop even where fold limbs dip in the same direction (Fig. 9i and j). As the interlimb angle of folds reduces, the acute angle measured between conjugate shear fractures becomes larger, suggesting fractures may have undergone rotation as fold limbs tighten and become sub-parallel to one another (Fig. 9e–j). Such folds are typically E to NE trending, although it is important to note that the shear fractures maintain a general NW–SE strike irrespective of the orientation of the associated fold hinge (Fig. 9e–j). Shear fracture intersection lineations are thus consistently NW–SE trending and may therefore become oblique to the fold hinge. In some cases, conjugate fractures only occur on the upper limb of the fold and the fractures terminate at internal fold detachments (Fig. 10a–d).

Where multiple phases of folding generate fold interference patterns (see Alsop and Marco, 2013), then the shear fractures form axial–planar to the F_2 phase of Type 3 hook patterns. They also define conjugate patterns about the F_2 phase of Type 1 dome and basin refolds (Fig. 10e and f). These relationships demonstrate that

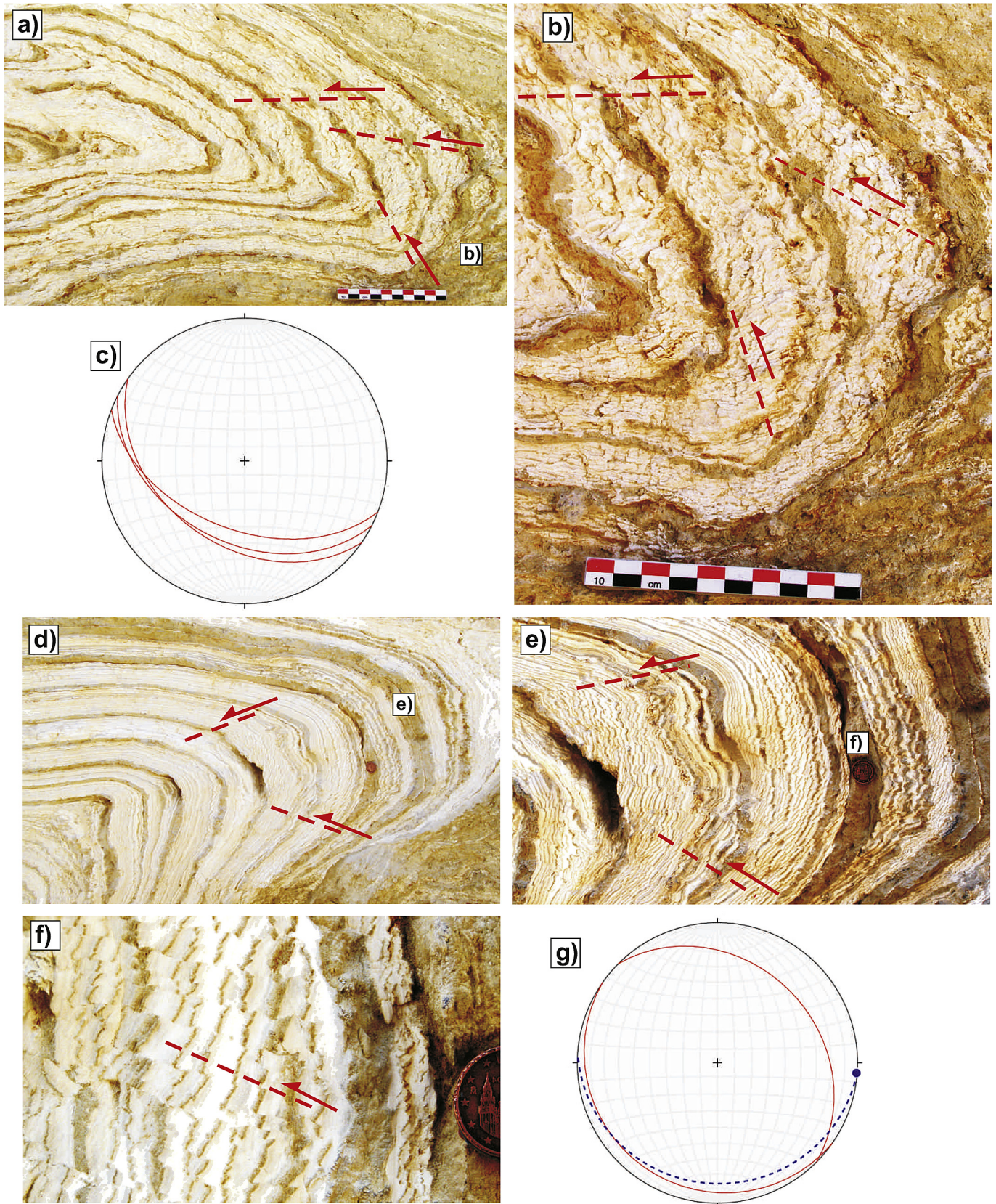


Fig. 8. Photographs and associated stereonets of pre-folding shear fractures. a) Fold hinge with shear fractures re-orientated around fold (b), resulting in the fractures dipping at variable angles to the SW (c). d–f) Shear fractures are reorientated around a fold hinge. Red dashed lines define orientation of fractures and arrow gives sense of movement. On stereonets c, g, fold hinge (blue circle), axial plane (dashed blue great circle) and variably orientated shear fractures (solid red great circles) are shown. Coin has a 15 mm diameter and scale bar is 10 cm. West is on the left and east on the right of the photographs. (For interpretation of the references to color in this figure legend, the reader is referred to the web version of this article.)

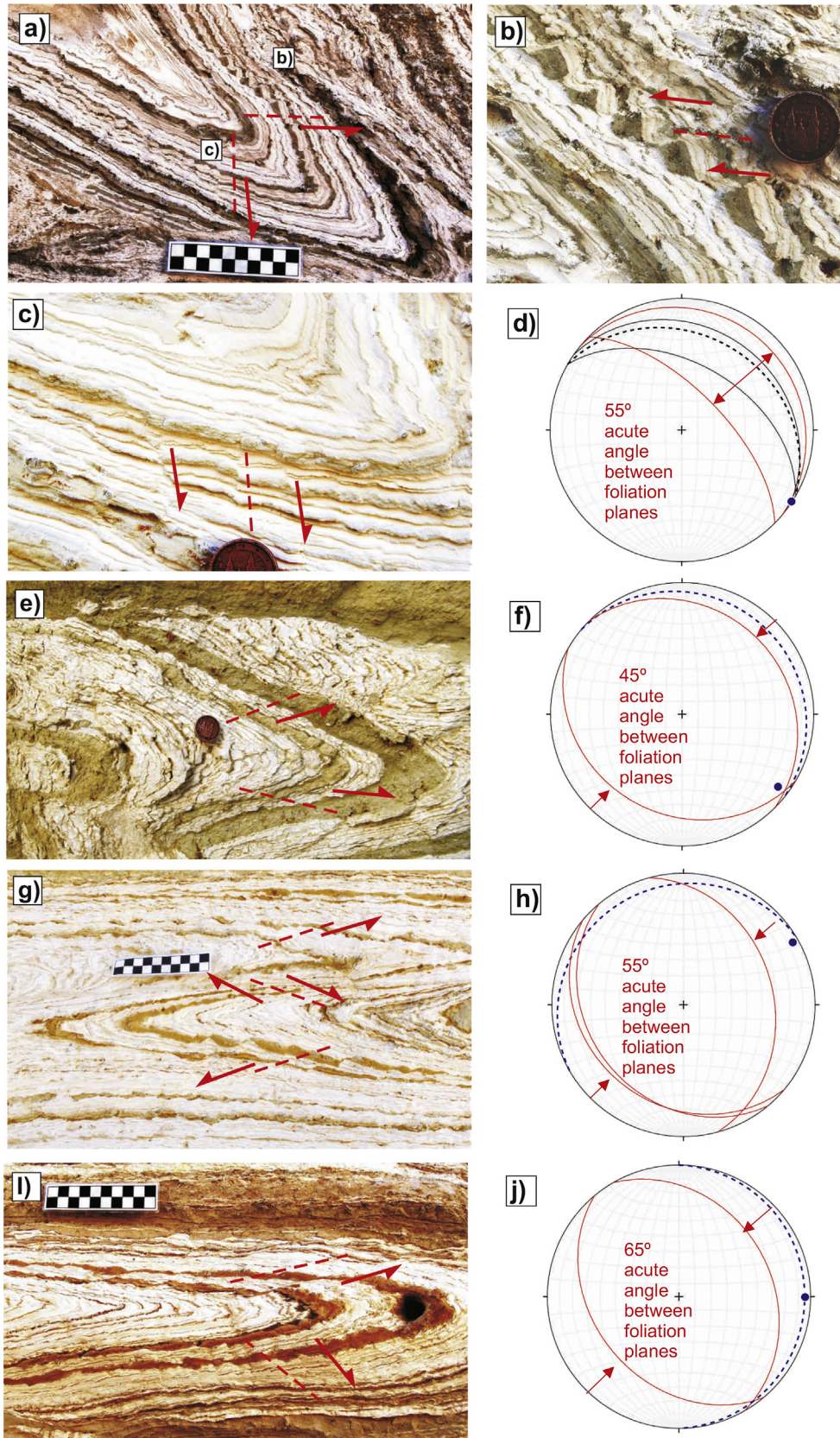


Fig. 9. a–j) Photographs and associated stereonet pairings of syn-folding shear fractures displaying reversals in kinematics across the axial plane of folds. b) and c) details of the upper and lower limbs of the fold in (a), (d) stereonet summary of structural data. Photographs and stereonet pairings (e, f), (g, h) and (i, j) show conjugate shear fractures that dip in opposite directions about folds and also display reversals in kinematics. The more open folds display the greatest angle between conjugate shear fractures (e, f), and as folds progressively tighten, the fracture angle sequentially reduces (g–j). Bedding (solid blue great circles), axial planes (dashed blue great circles), fold hinges (solid blue circles) and crenulation hinges (open blue circles) are shown on stereonets. The acute angle between fracture planes is measured normal to cleavage intersections. Coin has a 15 mm diameter and scale bar is 10 cm. West is on the left and east on the right of the photographs. (For interpretation of the references to color in this figure legend, the reader is referred to the web version of this article.)

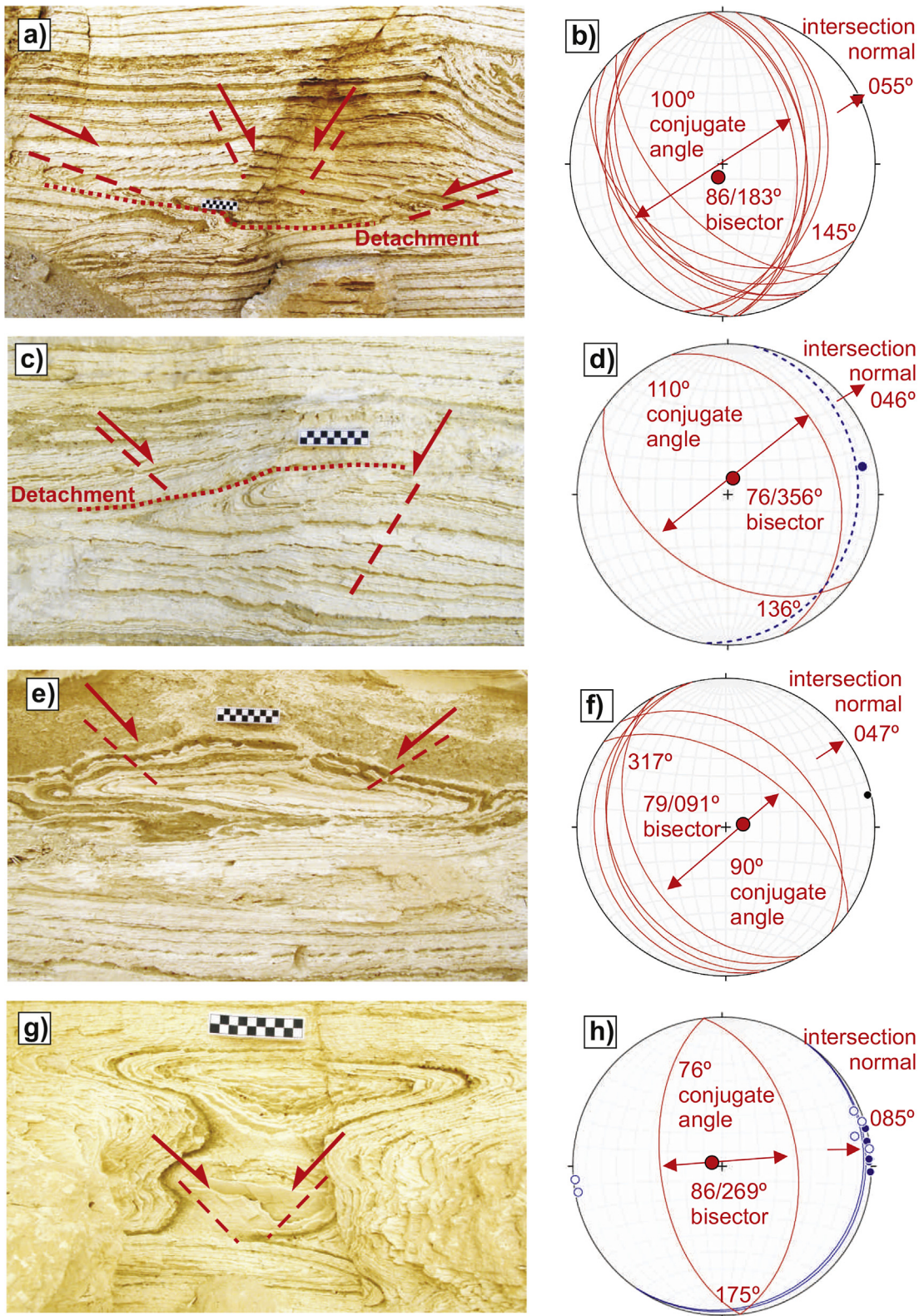


Fig. 10. a–f) Photographs and associated stereonet pairings of syn-folding shear fractures displaying conjugate patterns across the axial plane of folds. g–h) Photographs and associated stereonet pairings of post-folding shear fractures that overprint an eye-fold. Axial planes (dashed blue great circles), fold hinges (solid blue circles) and crenulation hinges (open blue circles) are shown on stereonets. Scale bar is 10 cm. West is on the left and east on the right of the photographs. (For interpretation of the references to color in this figure legend, the reader is referred to the web version of this article.)

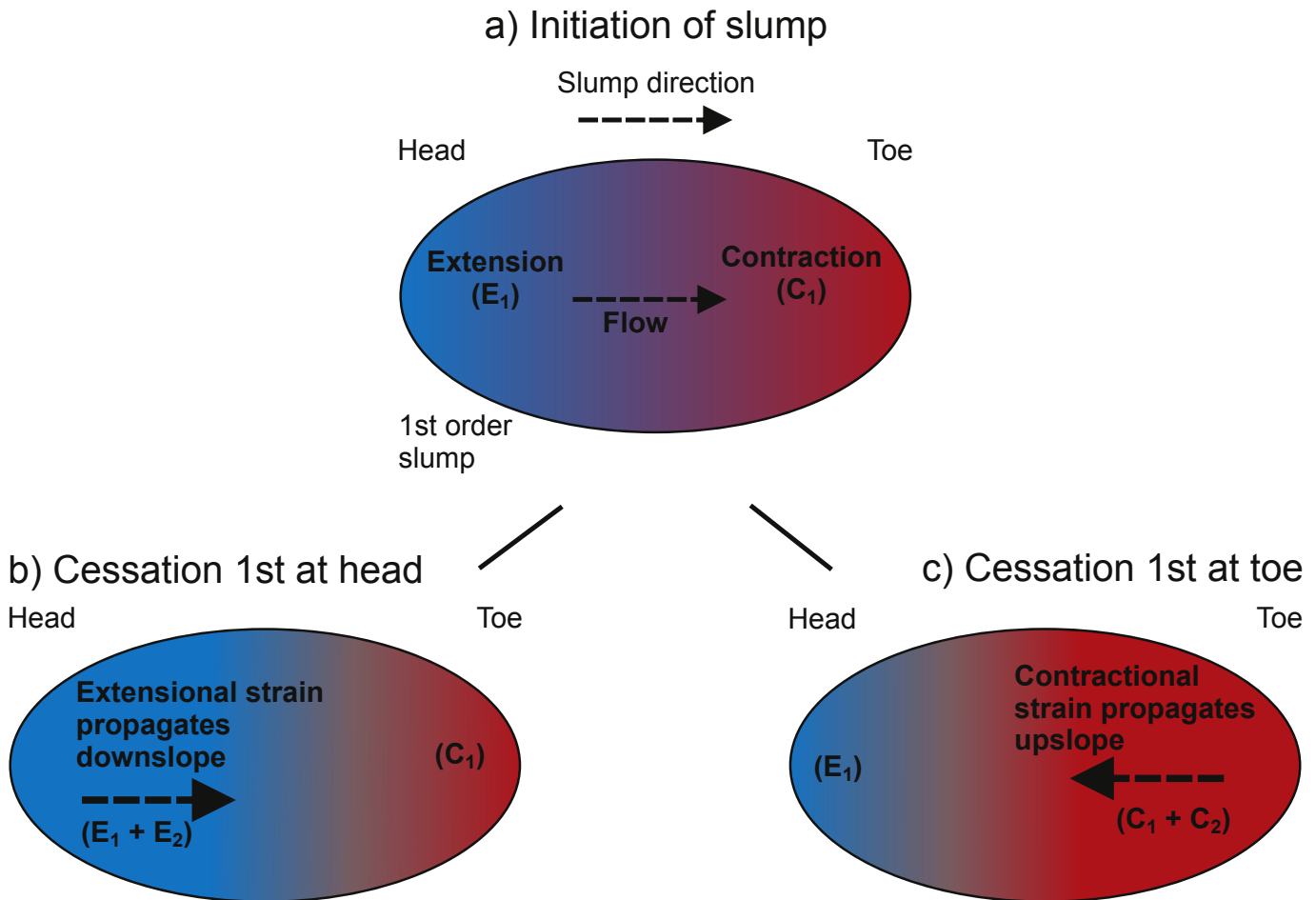


Fig. 11. Schematic dislocation cells associated with initiation (a) and subsequent cessation (b, c) of single-cell flow within slumps (see Farrell, 1984). Extensional (E_1 in blue) and contractional (C_1 in red) domains developed during initiation of the slump (a) are subsequently overprinted during cessation by either (b) extensional structures (E_2) propagating downslope from the head or (c) contractional structures (C_2) propagating upslope from the toe. (For interpretation of the references to color in this figure legend, the reader is referred to the web version of this article.)

shear fractures can form rapidly before associated folds are truncated by overlying erosive surfaces that are interpreted to develop during the same event (Alsop and Marco, 2012b). This inference confirms the genetic and temporal link between the shear fractures and folds.

6.3. Post-folding shear fractures

Foliation that overprints, and displays the same orientation and kinematics on both limbs of a fold, is typically considered as later than that fold in metamorphic terranes. Within the Lisan Formation, shear fractures may display the same orientation and kinematics on both limbs of folds or around eye fold patterns, suggesting that they formed after the folds (Fig. 10g and h). In addition, shear fractures can form axial-planar to the later folds (F_2) in refold patterns indicating that they postdate one set of folds but are syn-the second. The absence of shear fractures in the overlying undeformed strata constrains the time of fracture formation, and indicates that they formed as part of the slumping process when the folds were already fully developed.

In summary, the development of shear fractures on the limbs of folds with specific orientations suggests that they formed after the fold was created and only where the limbs were favourably orientated (Fig. 10g and h). Fold limbs that are parallel to shear fractures show no evidence of fracturing, whereas fold limbs at high angles are cross cut by numerous fracture planes. In other

instances, shear fractures form conjugate patterns around fold hinges (Fig. 10e, f), suggesting that they may be intimately related to creation of these folds via multiple deformation phases. Shear fractures cut adjacent crenulation cleavage indicating that the shear fractures locally developed later.

It should be noted that the amount of extension observed via normal faults or shear fractures within the slumps of the Lisan Formation, does not appear to be equivalent to the amount of contraction accommodated by folds and thrusts, as suggested in the original models of Farrell (1984) (see section 2). This disparity may simply reflect the distribution of exposure, with the up slope regions where extension would be expected to dominate being not as well exposed or incised as downslope areas, where contractional foliations and folds are observed. Different timing relationships exist between extensional shear fractures and contractional folds, and we believe it is therefore important to reconsider the general models of flow within slump systems. In particular, we consider how such fold and foliation patterns may be incorporated into both existing and new models of deformation within slump-sheets.

7. Models of flow within slump systems

The idea of an individual slump being modelled as a single large flow cell with extension at the head balanced by contraction at the toe has been established within the literature for more than 40 years (e.g. Lewis, 1971; Hansen, 1971), and was developed further

by the seminal work of Farrell (1984) (Fig. 11a). Although this elegant concept, that we here term the single-cell flow model as it is applied to the whole slump system, may provide a useful first-order approximation at the scale of seismic resolution, the detailed reality of slump systems observed at outcrop is frequently interpreted as more complex (see Gawthorpe and Clemney, 1985; Webb and Cooper, 1988; Martinsen and Bakken, 1990).

7.1. Traditional dislocation models of single-cell flow within slumps

Farrell (1984) applied a dislocation model to slumps, whereby deformation could be interpreted as being controlled by a large single-cell flow model. Thus, deformation would initiate along a decollement from a single point of failure, with contractional strain developing where the dislocation propagates in the same direction as the downslope slip direction, while extensional strain forms where the dislocation propagates in the opposite direction to the slip direction. Farrell (1984, p.728) also noted that fold vergence is generally controlled by, and in the same direction, as failure propagation, with contractional structures forming convex downslope map patterns, while extensional features are concave downslope (Fig. 1). This model accounted for the general strain pattern during slump initiation, where early extension (E_1) is focussed upslope of the initial point of failure in the slump, whereas contraction (C_1) dominates in the downslope toe area (Figs. 1 and 11a). Farrell (1984) also recognised that sequential velocity changes during translation of the slump may cause strain to propagate through the sediment and “superimpose strain on that already present” although no further details were provided.

If a slump first ceases or reduces movement at the head, then Farrell (1984) suggested that a second, late extensional strain wave (E_2) related to this cessation propagates down the slump system (Fig. 11b). This anti-dislocation would lead to extension related structures such as normal faults or extensional shear fractures postdating and therefore overprinting earlier translation related folds and fabrics within the slump (see Alsop and Marco, 2011) (Fig. 11b). These extensional features would generally dip in the downslope slip direction (Farrell, 1984, Fig. 8b). As the extensional strain wave (E_2) propagates down the slump from its head, then it is likely to overprint and/or reactivate existing normal faults generated within the extensional domain during the original initiation of the slump (E_1) i.e. $E_2 > E_1$ (Fig. 11b). Conversely, the single-cell flow model of Farrell (1984) predicts that a contractional strain wave (C_2) will propagate back up the slope through the slump-sheet if movement ceases first at the downslope toe (Fig. 11c). Although this strain wave propagates upslope, the vergence of associated folds and thrusts is still considered to be downslope, and existing contractional structures generated during initiation (C_1) may be reactivated and further tightened ($C_2 > C_1$). As such, deformation related to slump cessation will tend to simply reinforce the existing patterns of either extensional strain at the head of the slump ($E_2 > E_1$) or contractional strain at the toe ($C_2 > C_1$) (Fig. 11b and c).

In the present study, extensional shear fractures form a variety of pre-, syn- or post- folding relationships, indicating that the reality of slumps may be far more complex. Importantly, the pre, syn or post fracture folds display a similar range of geometric properties such as fold tightness, indicating that a simple relationship does not exist between fold style and timing of fracture development.

7.2. A new model of multi-cell flow within slumps

We here propose an alternative model that builds on Farrell's (1984) traditional ideas of deformation patterns within single-cell flows. We suggest that large (first-order) slumps are composed of a number of smaller (second-order) flow cells

developed during translation of the slump. This multi-flow cell model is based on the idea that flow cells are transient features that may locally interact and overprint one another during a single progressive deformation associated with slump translation. The idea that deformation generated during translation may be composed of a series of transient flow cells is long established in the literature relating to highly strained rocks at the base of metamorphic thrust-sheets (e.g. Coward and Potts, 1983; Holdsworth, 1990; Alsop and Holdsworth, 1993, 2002, 2007; Alsop et al., 2010; Xypolias and Alsop, 2014). Indeed, Farrell (1984, p.733) noted that sequential velocity changes may occur during translation, but did not consider this idea further.

Within any multi-cell flow system, second-order perturbations in flow during translation of the slump may relate to either a relative increase in velocity compared to the background resulting in surging flow (Fig. 12a), or alternatively a relative decrease in velocity compared to background to create slackening flow cells (Fig. 12b) (Alsop and Holdsworth, 2002, 2007). Within surging flow cells, extensional faults and fabrics dip in the flow direction, and form at the upslope head of the cell in domains of accelerating flow (Fig. 12a). Contractional folds and thrusts verge in the flow direction and form in regions of decelerating flow at the downslope toe of the cell (Fig. 12a). The degree of deformation increases towards areas of greatest relative acceleration or deceleration in flow velocity, frequently resulting in contractional structures becoming more intense towards the downslope toe (Fig. 12a). Clearly, any slumped unit is marked by an overall increase in downslope velocity relative to the adjacent unmoved sediments, and is therefore defined by surging flow on a gross scale. The overall deformation patterns in surging flow are thus equivalent to those developed during initiation of failure in single-cell flows (Farrell, 1984).

Within slackening flow cells, a relative decrease in cell velocity compared to the background flow results in a mirror-image configuration when compared to surging flow (e.g. Holdsworth, 1990; Alsop and Holdsworth, 2002, 2007) (Fig. 12b). Thus, contractional folds and thrusts verge in the flow direction and form in regions of decelerating flow now developed at the upslope head of the cell (Fig. 12b), whereas extensional faults and fabrics dip in the flow direction, and form at the downslope toe of the cell in domains of accelerating flow (Fig. 12b) (Alsop and Holdsworth, 2002). Once again, the degree of deformation increases towards areas of greatest relative acceleration or deceleration in flow velocity, frequently resulting in contractional structures becoming more intense towards the upslope head (Fig. 12b).

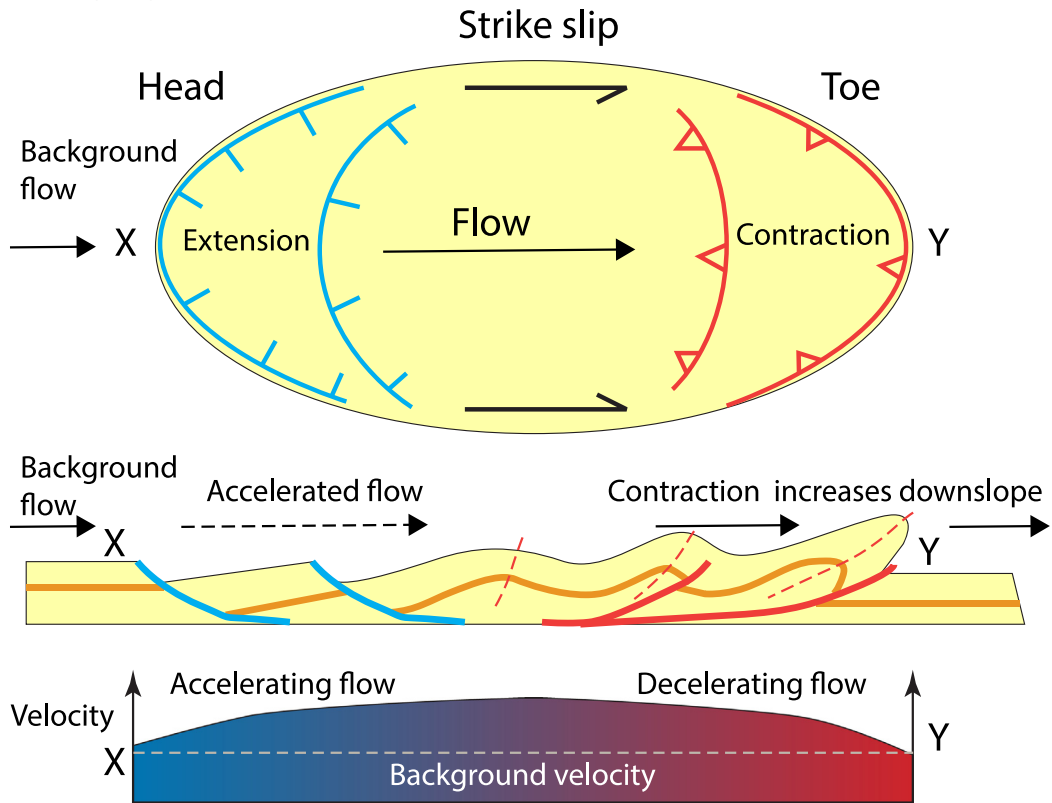
In addition to models of surging or slackening flow cells, new second-order transient flow cells may develop either further downslope or upslope of the existing perturbation. Clearly, older flow cells may be partially or wholly overprinted by new cells (e.g. Coward and Potts, 1983). Within this overall multi-cell flow model, we can therefore generate four potential end member scenarios during slump translation (Fig. 13). These will have distinct spatial relationships associated with differing overprinting patterns of deformation (Fig. 13). For instance later extension (E_2) may cut earlier contractional features (C_1) resulting in $E_2 > C_1$ overprinting relationships in either an upslope or downslope direction.

In addition to these end members, surging and slackening flow cells could directly overprint one another in an upslope or downslope direction. This behaviour will typically result in like on like superimposed deformation (i.e. $C_2 > C_1$ or $E_2 > E_1$) that in reality may be difficult to differentiate.

8. Discussion

We have shown above that grain-shape fabrics and crenulation cleavages are axial-planar to coeval slump folds, and are

a) Surging Flow



b) Slackening Flow

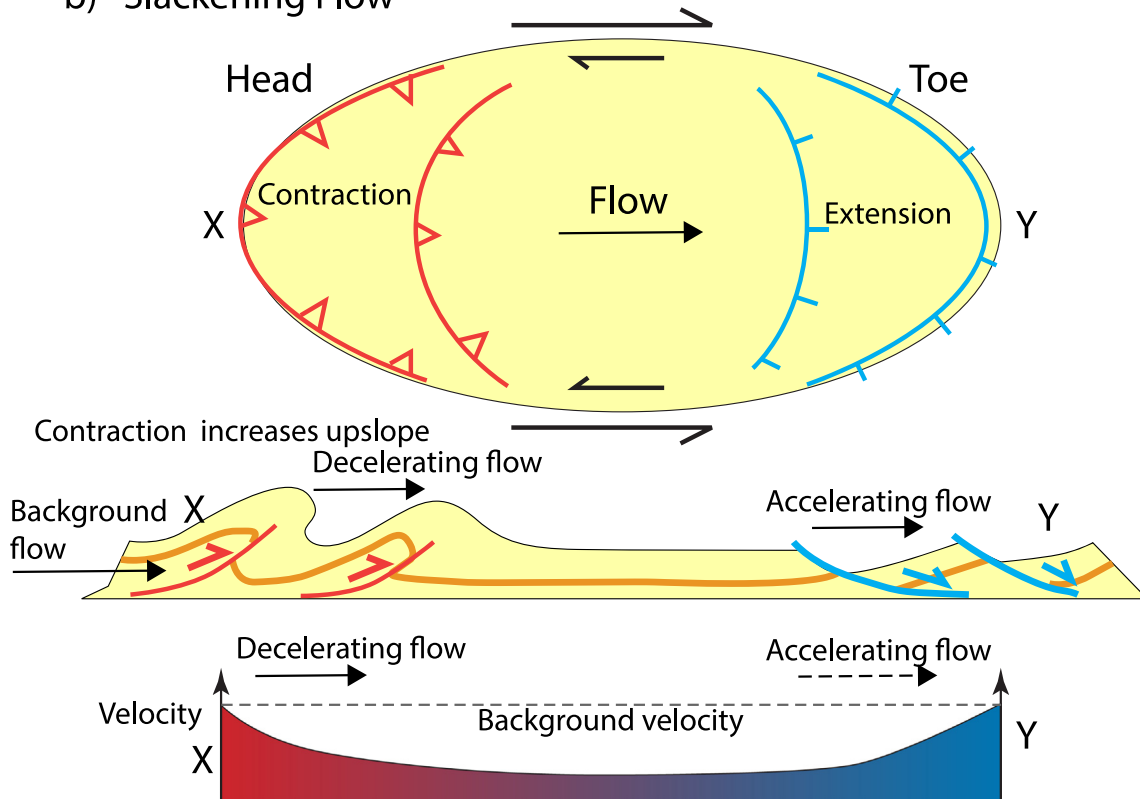


Fig. 12. Schematic maps and associated cross sections across second-order flow cells associated with (a) surging flow and (b) slackening flow developed during translation of the slump above a detachment. Length of arrows represents relative velocity in flow cells when compared to background flow, and this relationship is also illustrated in schematic velocity profile graphs. Deformation intensifies towards areas of greatest acceleration/deceleration in flow velocity.

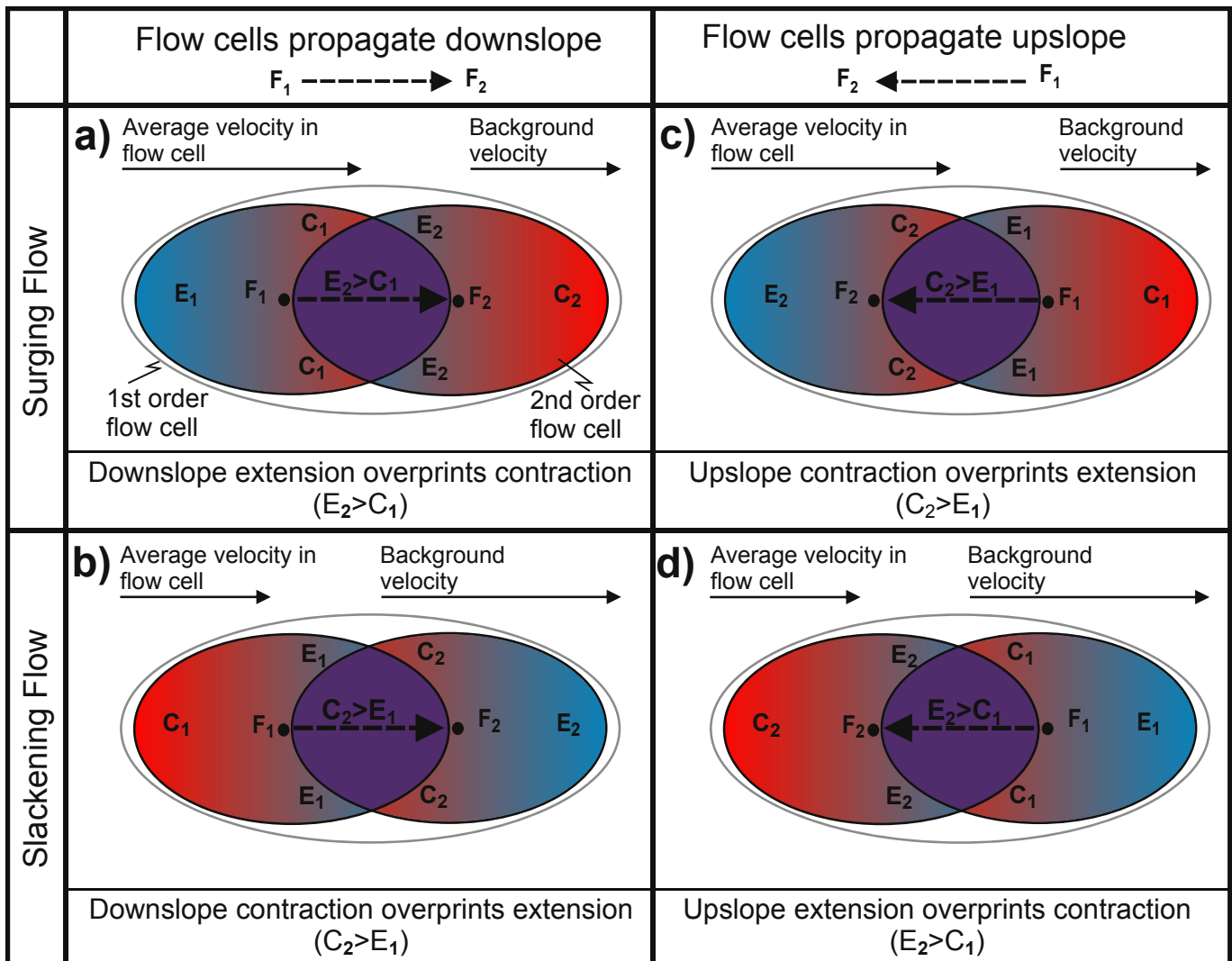


Fig. 13. Schematic maps of two transient second-order flow cells (F_1 and F_2) overprinting one another in an overall first-order flow cell associated with downslope slumping. Later extension (E_2) or contraction (C_2) associated with the second flow cell (F_2) is superimposed on earlier extension (E_1) and contraction (C_1) resulting in the range of potential overprinting scenarios (e.g. $C_2 > E_1$). Length of arrows represents relative velocity in flow cells when compared to background flow. a) *Downslope* $E_2 > C_1$: when new surging flow cells propagate in the flow direction, then later extensional structures (E_2) overprint earlier contractional features (C_1) in the downslope direction. b) *Downslope* $C_2 > E_1$: when new slackening flow cells propagate in the flow direction, then later contractional structures (C_2) overprint earlier extensional features (E_1) in the downslope direction. c) *Upslope* $C_2 > E_1$: when new surging flow cells propagate upslope against the flow direction, then later contractional structures (C_2) overprint earlier extensional features (E_1) in the upslope direction. d) *Upslope* $E_2 > C_1$: when new slackening flow cells propagate upslope against the flow direction, then later extensional structures (E_2) overprint earlier contractional features (C_1) in the upslope direction.

considered to be formed by contractional deformation. Shear fractures are penecontemporaneous with each slump, although in detail they may be pre-, syn- or post- associated slump folds, and are formed via extensional deformation. Although the fundamental issues we address concern the relationship of fabrics within slump folds to general models of slump systems, together with the use of foliation–fold relationships to distinguish slump folds from tectonic folds in lithified rocks, we start by discussing some of the more basic questions.

8.1. What are the different types of foliations and lineations that may form around slump folds?

Techniques established in classical structural analysis of metamorphic terranes (e.g. see Turner and Weiss, 1963; Ramsay, 1967) can be usefully employed in the analysis of slump structures where folds and foliations are formed. Grain-shape fabrics, crenulation

cleavages and extensional shear fractures that collectively form foliations create a range of intersection lineations that frequently parallel associated fold hinges. In some cases however, foliations and associated intersections are oblique and are observed to transect fold hinges. It should be noted that the structural relationships and fabrics described from this study develop in a matter of minutes and do not therefore represent punctuated separate events as is frequently interpreted in metamorphic rocks (see Alsop and Marco, 2013).

Although Elliot and Williams (1988, p.173) state that “it may not be possible for near-surface slump folds to have genetically related axial–planar PDO (preferred dimensional orientation) foliations”, the present study does indeed demonstrate an axial–planar relationship between grain-shape fabrics and slump folds. The presence of axial–planar grain-shape fabrics may not therefore be used to discriminate tectonic folds from slump folds in lithified rocks.

8.2. What are the relative timing relationships between foliations and slump folds?

Where shear fractures develop pre-folding, the fractures are observed in fold hinges where they display normal geometry on the upper fold limb and apparent reverse (contractional) displacement on the lower limb, where the direction of fracture dip has reversed. Their distribution in hinges and short limbs is inferred to result from the hinge migrating and wrapping the shear fracture around itself. Rotation of pre-fold fractures results in aragonite laminae within microlithons becoming markedly oblique to mud-rich layers upon which the spaced cleavage is considered to detach. The pre-folding shear fractures may be reactivated during folding thereby increasing obliquity of the laminae to mud-rich detachments, and intensifying the foliation.

Where shear fractures are syn-folding, they are observed to abruptly switch orientations and kinematics between the upper to lower fold limbs. This reversal in geometry occurs even when the fold limbs dip in the same direction. This consistency of geometry indicates that displacement on the fractures relates to kinematics of individual folds, rather than gravity-driven compaction, where fold limbs dipping in the same direction would be expected to display similar kinematics across foliation planes.

The relatively uniform NW–SE strike of syn-folding shear fractures irrespective of the orientation of the associated fold hinges suggests that (a) shear fractures formed relatively late in the folding process after any rotation of fold hinges towards the flow direction; or (b) the variable orientation of fold hinges is a consequence of folds initiating in a range of orientations, perhaps during differential shear, and the shear fractures were integral to this process. As fold tightness and axial–planar attitude do not vary with fold orientation then folds *initiating* in a variety of orientations (option b) may be more realistic in this case.

In summary, the observation that recumbent folds are associated with axial–planar shear fractures defining a foliation that fans about the fold hinge confirms that shear fractures are not simply a compaction related phenomena fortuitously parallel to the fold. In addition, the range of timing relationships developed between shear fractures and folds in the same slump-sheet forces us to carefully evaluate existing models of slumping.

8.3. What are the kinematics associated with sedimentary foliation development?

A range of mechanisms exist to create folds with associated foliations, which have been studied in detail across a variety of settings and rock types (see [Hudleston and Treagus, 2010](#); [Fossen, 2010](#), for general reviews). These mechanisms result into two broad categories of folds. In passive folds, layering such as bedding plays no part in the folding process and simply acts as a marker to define the fold shape. In these situations, the shear sense will be unaffected by layering and in most cases, is expected to remain constant around the fold and across its axial surface. In active folding, however, the layering has a rheological significance influencing the mechanical development of the fold. In these situations, the shear sense will reverse across the axial surface (see summary in [Alsop and Holdsworth, 2012](#)).

[Smith \(2000\)](#) undertook a detailed analysis of crinoid ossicles that had been variably offset within slump folds, and used this study to invoke flexural shear as a mechanism by which such folds evolved. Flexural shear is an active fold mechanism that involves shear being distributed within the different folded layers, and increases from zero at the hinge of the fold to a maximum value at the inflection point on each fold limb (see [Fossen, 2010](#), p.232). Importantly, the sense of shear reverses across the axial plane, such

that movement on layer-parallel detachments (i.e. weak bedding surfaces) should be directed out of the fold core and towards the outer folded layers. Within the Lisan Formation, the reversal in syn-folding shear fracture orientation and kinematics on crossing the axial plane of folds, together with the absence of fracture planes in the hinge of the fold, is consistent with flexural shear folding. In addition, bedding-parallel shear strain within the layers is shown by (a) the listric geometry of individual shear fracture planes as they rotate into mud-rich horizons; (b) back-rotation of aragonite-rich microlithons as displacement occurs; and (c) overall bulk kinematics indicating movement of hinges out of the fold core as per classical models of flexural shear folding.

Displacement may be modelled in terms of listric dominos, such that the bulk sense of shear around the fold is for the outer layers to be slipping/shearing away from the inner layers as the fold tightens. Similar reversals in kinematics around slump folds have been shown by [Farrell and Eaton \(1988, their Figs. 7a and 8\)](#). The shear fractures resemble shears generated in argillaceous sediments during experiments undertaken by [Maltman \(1977, 1987\)](#). [Elliot and Williams \(1988\)](#) were however critical of the assumptions concerning experimental parameters and suggested that they were “not conditions that would be found in natural sediments” as they represented conditions that were too deep for slump systems. The results generated are nonetheless similar to the natural examples we have described from slumps in the Lisan Formation.

In summary, the observations noted above collectively indicate that the slump folds within the Lisan Formation were not entirely passive, but rather underwent a degree of active folding during flexural shear. The mechanical significance of bedding during deformation is also supported by the development of buckle fold geometries during slumping (e.g. [Alsop and Marco, 2011](#)).

8.4. What relationship, if any, does the orientation of foliation have with the slope?

The trend of contractional folds and the strike of extensional shear fractures broadly correspond to one another, and are parallel to the inferred SE (130°) strike of the palaeoslope ([Alsop and Marco, 2012a](#)). This relationship suggests that extension and contraction associated with foliation development are dominated by down-slope shearing. The bisector to conjugate shear fractures in the slumps is sub-vertical, reflecting the influence of gravity, while the normal to shear fracture intersections is NE-trending parallel to the dip of the palaeoslope ([Figs. 6 and 10](#)). This dominance of strike-parallel structures suggests that differential shear along the lateral margins of slumps does not generate significant oblique or dip-parallel structures (see [Alsop and Marco, 2011](#) for a full discussion). This inferred behaviour may partly reflect the length/width ratio of individual cells measured in the direction of flow, with some cells dominated by layer-parallel shear resulting in proportionally greater along strike extents and relatively limited differential shear at the margins (see [Alsop and Holdsworth, 2007](#)). The laminated layer-cake nature of lacustrine sediments such as developed in the Lisan Formation may encourage such geometries ([Alsop and Marco, 2013](#)).

In detail, the shear fractures and foliation remain parallel to the inferred strike of the slope, no matter what the orientation of the associated fold hinge. This consistent geometry may suggest that (a) shear fractures formed relatively late in the folding process when the fold system was locking up; or (b) fold hinges which are oblique to the strike have formed in that orientation, rather than undergoing significant rotation along with the fractures towards the downslope direction. The reversal in orientation and kinematics of shear fractures across slump folds indicates that they are an integral component that formed at the same time as the

slumping. We therefore prefer model (b) with some folds initiating at variable angles to slope. Debacker et al. (2009) mapped major zones of oblique folding that they interpreted as representing the lateral margins of slump-sheets in the Anglo-Brabant deformation belt of Belgium. However no such systematic patterns are traceable in the present study, possibly suggesting that any zones of oblique folding form only minor (metre-scale) systems.

8.5. Can foliation–bedding relationships be used to distinguish slump folds from tectonic folds in lithified rocks?

Folds are perhaps the most ubiquitous of structures generated during flow of material in a wide range of environments, including within ductile metamorphic terranes and slumping in unlithified sediments. The resulting folds may be geometrically identical to one another in each setting, and distinguishing the origin of such folds in ancient lithified rocks can therefore be problematic. The presence of an axial–planar foliation has been used to suggest that the folds developed in a lithified rock, and hence by tectonic origin. Elliot and Williams (1988, p.174) provide a review of criteria to distinguish soft-sediment folding from tectonic folds and note that it “remains to be demonstrated that axial–planar foliations may be formed during near-surface slumping.” However, some sub-horizontal foliations observed in slump folds have been interpreted as being created during subsequent sediment compaction that is superimposed on recumbent slump folds (see discussion in Maltman, 1994c). Crenulation cleavages were also observed in slump folds by Farrell and Eaton (1988, p.569). However, these authors could not identify steeply dipping pervasive fabrics parallel to the axial planes of upright folds that would conclusively demonstrate that the crenulation fabrics were not the product of compaction.

Within the Lisan Formation, we interpret the grain-shape fabric defined by aragonite fragments as having formed by the whole-body rotation of the aragonite fragments during the slump folding of the mud-rich layer (section 5.1.1). Thus, aragonite fragments maintain their depositional bedding-parallel orientations on the limbs of the folds, whilst the aligned fragments become increasingly oblique to bedding and parallel to the axial plane of the folds in the hinge area (e.g. Fig. 4a and b). We do not consider this fabric to be formed via later compaction as: (a) the fabric itself can be inclined at significant angles of up to 28° from the horizontal; (b) the fabric is parallel to adjacent crenulation cleavages and shear fractures that demonstrably pre-date overlying erosive surfaces that truncate folds; and (c) overburden is too thin (typically <8 m) to generate significant compaction. These thicker mud-rich layers containing aragonite fragments typically act as weaker horizons during deformation and were interpreted as containing significant water (e.g. Alsop and Marco, 2011, 2013). The presence of water within the weak mud layers would further facilitate rotation of aragonite fragments to create an axial–planar grain-shape fabric. Thus, although Elliot and Williams (1988, p.174) note that “the presence of an axial–planar preferred dimensional orientation (fabric) inclined to bedding might be one way of distinguishing tectonic folds from surface slump folds”, it appears that such fabrics may indeed be locally developed within undoubted slumps of the Lisan Formation.

In summary, we believe that partially consolidated sediment, which displays enough cohesion to define folds and thrusts, is also capable of preserving axial–planar fabrics (see discussion in Maltman, 1994c). The identification within this study, not only of cleavages and foliations within undoubted sedimentary slump folds, but also of distinct foliation–bedding vergence relationships, indicates that the presence or absence of foliation is not in itself a robust criterion to distinguish tectonic and soft-sediment folds.

8.6. How may the development of foliation be incorporated into models of flow?

The range of timing relationships between shear fractures displaying extensional offsets of bedding, and folding reflecting contraction may be interpreted in terms of either a) the traditional *single-cell flow model* (Farrell, 1984) where multiple phases of extension and contraction relate to initiation and subsequent cessation in a single large (first-order) flow cell, or b) the new *multi-cell flow model* where numerous small (second-order) flow cells collectively form part of a larger structure, but locally interact and overprint one another during translation (see section 7.2). We will now discuss evidence for these two models in greater detail.

8.6.1. Extension overprints contraction ($E_2 > C_1$)

Extensional shear fractures are seen to overprint, and therefore postdate contractional folds in slumps at Peratzim (Fig. 10g and h). The traditional *single-cell flow model* established by Farrell (1984) invokes an individual extensional strain wave, and suggests that the large (first-order) slump may have locked first at the head, causing extensional strain to propagate downslope and overprint the contractional folds at the toe during slump cessation (Fig. 11a and b) (Farrell, 1984; see Alsop and Marco, 2011). Farrell (1984) noted that extensional structures superimposed on contractional folds is the more common of the overprinting scenarios.

However, the lack of consistent overprinting relationships on the scale of the slump leads us to propose the alternative *multi-cell flow model* whereby two smaller (second-order) flow cells of slightly differing age have mutually interfered with one another during slump translation. In this case, contraction (C_1) at the toe of the earlier slump has extensional deformation (E_2) superimposed on it such that $E_2 > C_1$. This relationship could be achieved by a general down-slope migration of new second-order surging flow cells (Fig. 13a) or upslope migration of slackening cells (Fig. 13d). In the case of downslope propagation, loading created by contractional folding and thrusting at the leading edge of the earlier slump may lead to a local increase in fluid pressure in the underlying sediments thereby encouraging new flow cells to initiate further downslope. Earlier flow cells may thus provide a degree of structural inheritance and control for where subsequent cells develop (see section 8.6.5).

8.6.2. Contraction overprints extension ($C_2 > E_1$)

The observation that extensional shear fractures are folded and wrapped around folds indicates that they pre-date those folds, and suggests that local contraction overprints extension ($C_2 > E_1$) (Fig. 8) (see section 6.1). The *single-cell flow model* (Farrell, 1984) invokes an individual contractional strain wave during cessation, resulting in folds consistently overprinting and folding extensional fabrics. Such a scenario could be created by a large (first-order) slump undergoing cessation first at the toe (Fig. 11a and c) (see Farrell, 1984; Alsop and Marco, 2011). However, a range of fold and extensional shear fracture relationships are observed, and only limited evidence exists for later shortening related to cessation in the slumped units (see Alsop and Marco, 2011, 2013).

We therefore suggest that the alternative *multi-cell flow model*, where two second-order flow cells of slightly differing age have mutually interfered with one another during translation, may be more applicable in this case. In this scenario, contractional deformation (C_2) is superimposed on extension (E_1) at the head of the earlier slump i.e. $C_2 > E_1$. This relationship could indicate a general up-slope migration of new second-order surging flow cells as might be expected during retrogressive slope failure (e.g. Gardner et al., 1999) (Fig. 13c). Alternatively, contraction may overprint

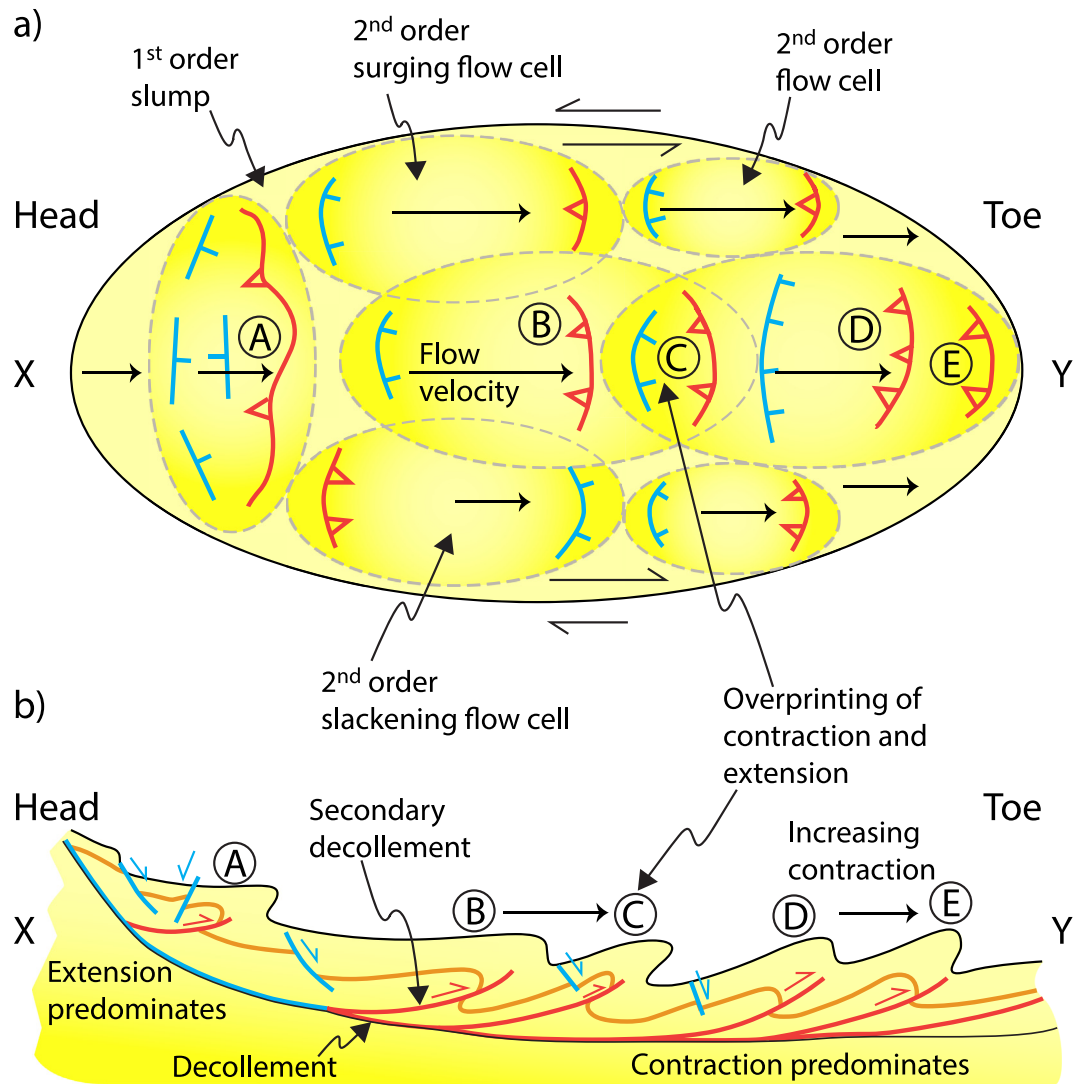


Fig. 14. Schematic map (a) and X–Y section (b) through a flow perturbation in a first-order slump comprising second-order cells (dashed ellipses) developed during the translation of a slump above a decollement. The length of arrows represents flow velocity, with an increase in velocity (as compared to background) reflecting overall surging flow. The transient multi-cells interact with neighbouring cells resulting in contractional fold and thrusts (in red) and extensional faults and cleavages (in blue) locally overprinting one another during overall translation. Circled locations (A–E) allow structures to be correlated from map to section. (For interpretation of the references to color in this figure legend, the reader is referred to the web version of this article.)

extension ($C_2 > E_1$) where slackening flow cells propagate in a downslope direction (Fig. 13b).

8.6.3. Contraction overprints extension ($C_2 > C_1$)

Within the slumps at Peratzim, contractional folds may be superimposed on one another ($C_2 > C_1$) resulting in classic Type 1 (dome and basin), Type 2 (boomerang) or Type 3 (hook) fold interference patterns (Alsop and Marco, 2013). The single-cell flow model suggests that contractional strain is generated if the slump first undergoes cessation at the toe, and this contractionally overprints the older folds and thrusts at the toe (Fig. 11c). The multi-cell flow model explains $C_2 > C_1$ overprinting by surging and slackening flow cells locally overprinting one another during either downslope or upslope propagation. The superposition of two unlike flow cells could also explain $E_2 > E_1$ relationships, although this case has not been identified in the present study and may be the most difficult to distinguish in the field.

In summary, the sporadic nature of the contractional overprint observed in the present study indicates that wholesale locking-up

of a large (km-scale) single-flow cell has not taken place. Where outcrop-scale examples of structures are observed, they are marked by increasing contraction at the downslope toe and extension at the upslope head of the local slump reflecting localised surging flow (Fig. 12a and b). We therefore prefer the multi-cell flow model, where local (second-order) variations in flow affect overall slump translation. In such a scenario, numerous metric and decametric flow cells interact with one another to create the range of overprinting patterns that are locally observed (Figs. 13 and 14).

8.6.4. Predictions of the multi-cell flow model

In general, the multi-cell flow model predicts a number of relationships including

- a) Second-order flow cells marked by zones of local contraction and extension may develop anywhere within the larger first-order flow cell, although contraction will still predominate at the toe and extension at the head of the slump (Fig. 14);

- b) Second-order flow cells can result in significant overprinting in areas where flow cells overlap and interfere with one another. The products of interference may develop anywhere within the first-order slump (Fig. 14) and are not restricted to the toe or head region as is typical in the cessation stage of the traditional single-cell flow model (Fig. 11b);
- c) Second-order flow cells develop during translation of the slump, whilst the single-cell flow model predicts that most deformation occurs during the initiation and cessation of the slump, thereby resulting in differing fold and fabric relationships; and
- d) Second-order flow cells may accommodate areas of accelerated surging flow as well as domains marked by an overall decrease in relative velocity associated with slackening flow (Figs. 13 and 14). Areas of slackening flow are not compatible with the single-cell flow model, which is entirely based on increased velocity compared to background flow.

The relationships described above may become more complex if:

- a) Individual second-order cells overprint larger areas of one another resulting in sets of either extensional ($E_1 + E_2$) or contractional ($C_1 + C_2$) structures directly coinciding with one another.
- b) Individual second-order surging and slackening flow cells overprint one another resulting in coincidence of either extensional ($E_1 + E_2$) or contractional ($C_1 + C_2$) structures.
- c) Individual second-order cells contain additional structures generated during cessation of movement within that particular cell (see Farrell, 1984; Alsop and Marco, 2011).
- d) Individual second-order cells and associated decollements are formed at different levels within the same slump-sheet. Models of non-coaxial dominated deformation along a basal decollement being overlain by greater components of pure shear have been developed in slumps (e.g. Webb and Cooper, 1988). However, such models are not useful if a series of vertically stacked decollements are formed, resulting in non-coaxial deformation associated with the decollement of an overlying cell interacting with the pure shear component of an underlying and synchronous system (Fig. 14).

8.6.5. Controls and consequences of the multi-cell model

The multi-cell model is based on the development of second-order flow cells during translation of the slump. Factors that are likely to influence local velocity within the slump, and hence the creation of second-order perturbations include (a) local variations in lithology and/or geometry of stratigraphic units such as channels; (b) local variations in fluid pressure both within the slump and within underlying sediments; (c) local variations in slope and/or orientation of the decollement below the slump (see Farrell, 1984; Alsop and Marco, 2011). Although these factors may display variations before initiation of slumping, they also have the potential to continually evolve during the actual slump translation. Thus, slumps may rework and mix sediments as they develop, or result in local increases or decreases in fluid pressure as thrust and folded slump-sheets increase overburden loading (e.g. see Strachan and Alsop, 2006). Variations in bathymetry may be created by zones of contraction and extension, which then influence subsequent slump translation and development. Areas that are overthickened and unstable will tend to extend and thin, whereas extended areas forming bathymetric lows will tend to pond sediments. Many of these potential influences are similar to those invoked in critical wedge models, as the gravity-driven slump strives for dynamic equilibrium.

9. Conclusions

- a) Multiple foliation sets generate a range of lineations and overprinting relationships around slump folds in the Lisan Formation of the Dead Sea Basin. Contractional deformation results in grain-shape fabrics and crenulation cleavages that are axial–planar to slump folds, and are developed in mud-rich and aragonite-rich horizons respectively. Extensional deformation results in foliations marked by shear fractures, which can be pervasive in aragonite-rich beds. Shear fractures may however locally steepen and become more widely spaced when passing through thin mud-rich units, suggesting these units were more competent at this time.
- b) Folds and fabrics, including crenulation cleavage and shear fractures, are broadly syn-tectonic with respect to each slump. Within individual slumps however, extensional shear fractures may be pre, syn or post local folding reflecting the dynamic interplay between contraction and extension. These relationships suggest that extension and contraction are more spatially and temporally heterogeneous than in classical models of slump systems.
- c) The shear fractures that are axial–planar to slump folds display extensional offset with respect to bedding, and systematic kinematics in relation to folds. The overall sense of kinematic reversal around folds is consistent with a flexural shear component to folding, and demonstrates that slump folds underwent a component of active folding.
- d) The SE-striking shear fractures display a direct relationship with the attitude of the slope that controlled slumping. Variable fracture dips towards both the NE and SW are consistent with an overall domino system, such that SW-dipping extensional fractures relate to overall NE-directed gravity-driven movement down the palaeoslope of the Dead Sea Basin.
- e) The use of foliation–bedding relationships to distinguish sedimentary and tectonic folds is fraught with difficulty. The recognition within this study of axial–planar grain-shape fabrics and distinct foliation–bedding relationships demonstrates that the presence or absence of foliation cannot be used to differentiate tectonic folds formed in lithified rock from those folds generated via slumping.
- f) The development of foliation is integral to models of flow within slump systems. Classic models of slumping predict extension at the head of slumps with normal faults dipping in the downslope direction. Within the study, extensional deformation is pervasively accommodated throughout the slumped mass by variably dipping extensional shear fractures, indicating that the classical models may be usefully updated.

To conclude, the variety of relationships observed between extensional shear fractures and folds from within the same slump-sheet leads us to propose that individual slumps are composed of a series of second-order flow cells. We thus revise the traditional single-cell dislocation model that focuses on structures generated during the initiation and cessation of the first-order slump, to develop a *multi-cell flow model* that concentrates on second-order structures created during slump translation. The two models are not therefore mutually exclusive. The *multi-cell flow model* represents local areas of surging or slackening flow within the translating slump, that temporally and spatially interact with one another to create the range of relationships and fold/fabric scenarios noted above. The multi-cell model predicts that extensional and contractional structures may be superimposed on one another in any order and in any position within the overall slumped mass.

We suggest that the strict spatial (toe and head), temporal (initiation, translation and cessation) or uni-scalar (first-order) division of structures within traditional single-cell models of slump-sheets is in general too simple and inadequate when compared to the reality observed below the scale of an entire slumped body.

Acknowledgements

We thank the Carnegie Trust for travel grants to IA, and the Israel Science Foundation for grant 1736/11 to SM. SM also thanks the Department of Earth Sciences at Durham University for hosting a visit and special cutting of a thin section (Fig. 3). The authors would like to thank Nigel Woodcock and Hugo Ortner for detailed reviews which improved the manuscript together with Bill Dunne for careful editorial handling.

References

- Aftabi, P., Rostaie, M., Alsop, G.I., Talbot, C.J., 2010. InSAR mapping and modelling of an active Iranian salt extrusion. *J. Geol. Soc. London* 167, 155–170.
- Agnon, A., Migowski, C., Marco, S., 2006. Intraclast breccia layers in laminated sequences: recorders of paleo-earthquakes. In: Enzel, Y., Agnon, A., Stein, M. (Eds.), *New Frontiers in Dead Sea Paleoenvironmental Research*, Geological Society of America Special Publication, pp. 195–214.
- Allen, J.R.L., 1984. *Sedimentary Structures, Their Character and Physical Basis*. In: *Developments in Sedimentology*, vol. 30. Elsevier, Amsterdam, p. 663.
- Alsop, G.I., Holdsworth, R.E., 1993. The distribution, geometry and kinematic significance of Caledonian buckle folds in the western Moine Nappe, northwestern Scotland. *Geological Magazine* 130, 353–362.
- Alsop, G.I., Cheer, D.A., Strachan, R.A., Krabbendam, M., Kinny, P.D., Holdsworth, R.E., Leslie, A.G., 2010. Progressive fold and fabric evolution associated with regional strain gradients: a case study from across a Scandian ductile thrust Nappe, Scottish Caledonides. In: Law, R.D., Butler, R.W.H., Holdsworth, R.E., Krabbendam, M., Strachan, R.A. (Eds.), *Continental Tectonics and Mountain Building: the Legacy of Peach and Horne*, Geological Society, London, Special Publications, vol. 335, pp. 253–272.
- Alsop, G.I., Carreras, J., 2007. Structural evolution of sheath folds: a case study from Cap de Creus. *J. Struct. Geol.* 29, 1915–1930.
- Alsop, G.I., Holdsworth, R.E., 2002. The geometry and kinematics of flow perturbation folds. *Tectonophysics* 350, 99–125.
- Alsop, G.I., Holdsworth, R.E., 2007. Flow perturbation folding in shear zones. In: Ries, A.C., Butler, R.W.H., Graham, R.D. (Eds.), *Deformation of the Continental Crust: the Legacy of Mike Coward*, Geological Society, London, Special Publications, vol. 272, pp. 77–103.
- Alsop, G.I., Holdsworth, R.E., 2012. The three dimensional shape and localisation of deformation within multilayer sheath folds. *J. Struct. Geol.* 44, 110–128.
- Alsop, G.I., Marco, S., 2011. Soft-sediment deformation within seismogenic slumps of the Dead Sea Basin. *J. Struct. Geol.* 33, 433–457.
- Alsop, G.I., Marco, S., 2012a. A large-scale radial pattern of seismogenic slumping towards the Dead Sea Basin. *J. Geol. Soc. London* 169, 99–110.
- Alsop, G.I., Marco, S., 2012b. Tsunami and seiche-triggered deformation within offshore sediments. *Sediment. Geol.* 261, 90–107.
- Alsop, G.I., Marco, S., 2013. Seismogenic slump folds formed by gravity-driven tectonics down a negligible subaqueous slope. *Tectonophysics* 605, 48–69.
- Bartov, Y., Steinitz, G., Eyal, M., Eyal, Y., 1980. Sinistral movement along the Gulf of Aqaba – its age and relation to the opening of the Red Sea. *Nature* 285, 220–221.
- Begin, Z.B., Ehrlich, A., Nathan, Y., 1974. Lake Lisan, the Pleistocene precursor of the Dead Sea. *Geol. Surv. Israel Bull.* 63, 30.
- Bell, C.M., 1981. Soft-sediment deformation of sandstone related to the Dwyka glaciation in South Africa. *Sedimentology* 28, 321–329.
- Bradley, D., Hanson, L., 1998. Paleoslope analysis of slump folds in the Devonian flysch of Main. *J. Geol.* 106, 305–318.
- Bull, S., Cartwright, J., Huuse, M., 2009. A review of kinematic indicators from mass-transport complexes using 3D seismic data. *Mar. Petrol. Geol.* 26, 1132–1151.
- Butler, R.W.H., Paton, D.A., 2010. Evaluating lateral compaction in deepwater fold and thrust belts: how much are we missing from Natures sandbox? *GSA Today* 20, 4–10.
- Corbett, K.D., 1973. Open-cast slump sheets and their relationship to sandstone beds in an Upper Cambrian flysch sequence, Tasmania. *J. Sediment. Petrol.* 43, 147–159.
- Coward, M.P., Potts, G.J., 1983. Complex strain patterns developed at the frontal and lateral tips to shear zones and thrust zones. *J. Struct. Geol.* 5, 383–399.
- Debacker, T.N., Sintubin, M., Verniers, J., 2001. Large-scale slumping deduced from structural and sedimentary features in the Lower Palaeozoic Anglo-Brabant fold belt, Belgium. *J. Geol. Soc. London* 158, 341–352.
- Debacker, T.N., van Noorden, M., Sintubin, M., 2006. Distinguishing syn-cleavage folds from pre-cleavage folds to which cleavage is virtually axial planar: examples from the Cambrian core of the Lower Palaeozoic Anglo-Brabant Deformation Belt (Belgium). *J. Struct. Geol.* 28, 1123–1138.
- Debacker, T.N., Dumon, M., Matthys, A., 2009. Interpreting fold and fault geometries from within the lateral to oblique parts of slumps: a case study from the Anglo-Brabant Deformation Belt (Belgium). *J. Struct. Geol.* 31, 1525–1539.
- Elliot, C.G., Williams, P.F., 1988. Sediment slump structures: a review of diagnostic criteria and application to an example from Newfoundland. *J. Struct. Geol.* 10, 171–182.
- Farrell, S.G., 1984. A dislocation model applied to slump structures, Ainsa Basin, South Central Pyrenees. *J. Struct. Geol.* 6, 727–736.
- Farrell, S.G., Eaton, S., 1987. Slump strain in the Tertiary of Cyprus and the Spanish Pyrenees. Definition of palaeoslopes and models of soft sediment deformation. In: Jones, M.F., Preston, R.M.F. (Eds.), *Deformation of Sediments and Sedimentary Rocks*, Special Publication of the Geological Society of London, vol. 29, pp. 181–196.
- Farrell, S.G., Eaton, S., 1988. Foliations developed during slump deformation of Miocene marine sediments, Cyprus. *J. Struct. Geol.* 10, 567–576.
- Fossen, H., 2010. *Structural Geology*. Cambridge University Press, Cambridge, UK, p. 463.
- García-Tortosa, F.J., Alfaro, P., Gilbert, L., Scott, G., 2011. Seismically induced slump on an extremely gentle slope (<1°) of the Pleistocene Tecopa paleolake (California). *Geology* 39, 1055–1058.
- Gardner, J.V., Prior, D.B., Field, M.E., 1999. Humboldt slide – a large shear dominated retrogressive slope failure. *Mar. Geol.* 154, 323–338.
- Garfunkel, Z., 1981. Internal structure of the Dead Sea leaky transform (rift) in relation to plate kinematics. *Tectonophysics* 80, 81–108.
- Garfunkel, Z., Ben-Avraham, Z., 1996. The structure of the Dead Sea basin. *Tectonophysics* 26, 155–176.
- Gawthorpe, R.L., Clemney, H., 1985. Geometry of submarine slides in the Bowland Basin (Dinantian) and their relation to debris flows. *J. Geol. Soc.* 142, 555–565.
- Gilbert, L., Sanz de Galdeano, C., Alfaro, P., Scott, G., Lopez Garrido, A.C., 2005. Seismic-induced slump in Early Pleistocene deltaic deposits of the Baza Basin (SE Spain). *Sediment. Geol.* 179, 279–294.
- Haase-Schramm, A., Goldstein, S.L., Stein, M., 2004. U-Th dating of Lake Lisan aragonite (late Pleistocene Dead Sea) and implications for glacial East Mediterranean climate change. *Geochim. Cosmochim. Acta* 68, 985–1005.
- Hansen, E., 1971. *Strain Facies*. Springer-Verlag, Berlin, p. 207.
- Holdsworth, R.E., 1990. Progressive deformation structures associated with ductile thrusts in the Moine Nappe, Sutherland, N Scotland. *J. Struct. Geol.* 12, 443–452.
- Hudleston, P.J., Treagus, S.H., 2010. Information from folds: a review. *J. Struct. Geol.* 32, 2042–2071.
- Hurst, A., Scott, A., Vigorito, M., 2011. Physical characteristics of sand injectites. *Earth-Sci. Rev.* 106, 215–246.
- Jackson, C.A.-L., 2011. Three-dimensional seismic analysis of megaclast deformation within a mass transport deposit: implications for debris flow kinematics. *Geology* 39, 203–206.
- Lee, H.J., Locat, J., Desgagnés, P., Parsons, J.D., McAdoo, B.G., Orange, D.L., Puig, P., Wong, F.L., Dartnell, P., Boulanger, E., 2007. Submarine mass movements on continental margins. In: Nittrouer, C.A., Austin, J.A., Field, M.E., Kravitz, J.H., Syvitski, J.P.M., Wiberg, P.L. (Eds.), *Continental Margin Sedimentation: from Sediment Transport to Sequence Stratigraphy*, Special Publication of the International Association of Sedimentologists, vol. 37. Blackwell Publishing, pp. 213–274.
- Lesemann, J.-E., Alsop, G.I., Piotrowski, J.A., 2010. Incremental subglacial meltwater sediment deposition and deformation associated with repeated ice-bed decoupling: a case study from the Island of Funen, Denmark. *Quat. Sci. Rev.* 29, 3212–3229.
- Levi, T., Weinberger, R., Aifa, T., Eyal, Y., Marco, S., 2006. Injection mechanism of clay-rich sediments into dikes during earthquakes: Geochemistry. *Geophys. Geosyst.* 7 (12), Q12009 doi:10.1029/2006GG001410.
- Lewis, K.B., 1971. Slumping on a continental slope inclined at 1–4°. *Sedimentology* 16, 97–110.
- Maltman, A.J., 1977. Some microstructures of experimentally deformed argillaceous sediments. *Tectonophysics* 39, 417–436.
- Maltman, A., 1981. Primary bedding-parallel fabrics in structural geology. *J. Geol. Society, London* 138, 475–483.
- Maltman, A., 1984. On the term soft-sediment deformation. *J. Struct. Geol.* 6, 589–592.
- Maltman, A., 1987. Shear zones in argillaceous sediments – an experimental study. In: Jones, M.F., Preston, R.M.F. (Eds.), *Deformation of Sediments and Sedimentary Rocks*, Special Publication of the Geological Society of London, vol. 29, pp. 77–87.
- Maltman, A., 1994a. *The Geological Deformation of Sediments*. Chapman & Hall, London, p. 362.
- Maltman, A., 1994b. Introduction and overview. In: Maltman, A. (Ed.), *The Geological Deformation of Sediments*. Chapman & Hall, London, pp. 1–35.
- Maltman, A., 1994c. Deformation structures preserved in rocks. In: Maltman, A. (Ed.), *The Geological Deformation of Sediments*. Chapman & Hall, London, pp. 261–307.
- Maltman, A., 1994d. Prelithification deformation. In: Hancock, P.L. (Ed.), *Continental Deformation*. Pergamon Press, pp. 143–158.
- Marco, S., Agnon, A., 1995. Prehistoric earthquake deformations near Masada, Dead Sea graben. *Geology* 23, 695–698.
- Marco, S., Weinberger, R., Agnon, A., 2002. Radial clastic dykes formed by a salt diapir in the Dead Sea Rift, Israel. *Terra Nova* 14, 288–294.

- Martinsen, O.J., 1989. Styles of soft-sediment deformation on a Namurian delta slope, Western Irish Namurian Basin, Ireland. In: Whateley, M.K.G., Pickering, K.T. (Eds.), *Deltas: Sites and Traps for Fossil Fuels*, Geological Society of London Special Publication, vol. 41. Geological Society London, London, pp. 167–177.
- Martinsen, O.J., 1994. Mass movements. In: Maltman, A. (Ed.), *The Geological Deformation of Sediments*. Chapman & Hall, London, pp. 127–165.
- Martinsen, O.J., Bakken, B., 1990. Extensional and compressional zones in slumps and slides in the Namurian of County Claire, Eire. *J. Geol. Soc. London* 147, 153–164.
- McClay, K.R., 1987. *The Mapping of Geological Structures*. Geological Society, London (Handbook).
- McClelland, H.L.O., Woodcock, N.H., Gladstone, C., 2011. Eye and sheath folds in turbidite convolute lamination: Aberystwyth Grits Group, Wales. *J. Struct. Geol.* 33, 1140–1147.
- Ortner, H., 2007. Styles of soft-sediment deformation on top of a growing fold system in the Gosau Group at Muttekopf, Northern Calcareous Alps, Austria: slumping versus tectonic deformation. *Sediment. Geol.* 196, 99–118.
- Passchier, C.W., Trouw, R.A.J., 2005. *Microtectonics*, second ed. Springer, p. 366.
- Phillips, C.A., Alsop, G.I., 2000. Post-tectonic clastic dykes in the Dalradian of Scotland and Ireland: implications for delayed lithification of sediments. *Geol. J.* 35, 99–110.
- Pisarska-Jamroz, M., Weckwerth, P., 2012. Soft-sediment deformation structures in a Pleistocene glaciolacustrine delta and their implications for the recognition of subenvironments in delta deposits. *Sedimentology* 60 (3), 637–665.
- Porat, N., Levi, T., Weinberger, R., 2007. Possible resetting of quartz OSL signals during earthquakes – evidence from late Pleistocene injection dikes, Dead Sea basin, Israel. *Quat. Geochronol.* 2, 272–277.
- Potter, P.E., Pettijohn, F.J., 1963. *Palaeocurrents and Basin Analysis*. Springer-Verlag, New York.
- Price, N.J., Cosgrove, J.W., 1990. *Analysis of Geological Structures*. Cambridge University Press.
- Ramsay, J.G., 1967. *Folding and Fracturing of Rocks*. McGraw Hill, New York, p. 568.
- Ramsay, J.G., Huber, M.I., 1987. *The Techniques of Modern Structural Geology*. In: *Folds and Fractures*, vol. 2. Academic Press.
- Smith, J.V., 2000. Flow pattern within a Permian submarine slump recorded by oblique folds and deformed fossils, Ulladulla, south-eastern Australia. *Sedimentology* 47, 357–366.
- Strachan, L.J., 2002. Slump-initiated and controlled syndepositional sandstone remobilization; an example from the Namurian of County Clare, Ireland. *Sedimentology* 49, 25–41.
- Strachan, L.J., 2008. Flow transformations in slumps: a case study from the Waitemata Basin, New Zealand. *Sedimentology* 55, 1311–1332.
- Strachan, L.J., Alsop, G.I., 2006. Slump folds as estimators of palaeoslope: a case study from the Fisherstreet Slump of County Clare, Ireland. *Basin Res.* 18, 451–470.
- Tobisch, O.T., 1984. Development of foliation and fold interference patterns produced by sedimentary processes. *Geology* 12, 441–444.
- Turner, F.J., Weiss, L.E., 1963. *Structural Analysis of Metamorphic Tectonites*. McGraw-Hill, New York.
- Waldron, J.W.F., Gagnon, J.-F., 2011. Recognizing soft-sediment structures in deformed rocks of orogens. *J. Struct. Geol.* 33, 271–279.
- Webb, B.C., Cooper, A.H., 1988. Slump folds and gravity slide structures in a lower Palaeozoic marginal basin sequence (the Skiddaw Group) NW England. *J. Struct. Geol.* 10, 463–472.
- Wetzler, N., Marco, S., Heifetz, E., 2010. Quantitative analysis of seismogenic shear-induced turbulence in lake sediments. *Geology* 38, 303–306.
- Williams, P.F., Collins, A.R., Wiltshire, R.G., 1969. Cleavage and penecontemporaneous deformation structures in sedimentary rocks. *J. Geol.* 77, 415–425.
- Woodcock, N.H., 1976a. Ludlow Series slumps and turbidites and the form of the Montgomery Trough, Powys, Wales. *Proc. Geologists Assoc.* 87, 169–182.
- Woodcock, N.H., 1976b. Structural style in slump sheets: Ludlow series, Powys, Wales. *J. Geol. Soc. London* 132, 399–415.
- Woodcock, N.H., 1979. The use of slump structures as palaeoslope orientation estimators. *Sedimentology* 26, 83–99.
- Xypolias, P., Alsop, G.I., 2014. Regional flow perturbation folding within an exhumation channel: a case study from the Cycladic Blueschists. *J. Struct. Geol.* in press.